Turkish Journal of Earth Sciences

Volume 28 | Number 1 Article 3

1-1-2019

Geochronological and geochemical constraints and origin of the Tavşanlı Zoneplutonic rocks (NW Turkey)

METİN BAĞCI

MEHMET DEMİRBİLEK

NURDANE İLBEYLİ

AHMET YILDIZ

YAŞAR KİBİCİ

TÜBİTAK

Turkish Journal of Earth Sciences

http://journals.tubitak.gov.tr/earth/

Research Article

Turkish J Earth Sci
(2019) 28: 60-84

doi:10.3906/yer-1712-25

Geochronological and geochemical constraints and origin of the Tavşanlı Zone plutonic rocks (NW Turkey)

Metin BAĞCI[1,*], Mehmet DEMİRBİLEK[2], Nurdane İLBEYLİ[3], Ahmet YILDIZ[1], Yaşar KİBİCİ[4]

[1]Department of Geological Engineering, Faculty of Engineering, Afyon Kocatepe University, Afyonkarahisar, Turkey
[2]Department of Geological Engineering, Faculty of Engineering, Dumlupınar University, Kütahya, Turkey
[3]Department of Geological Engineering, Faculty of Engineering, Akdeniz University, Antalya, Turkey
[4]Program of Construction Technician, Vocational School, Bilecik Şeyh Edebali University, Bilecik, Turkey

Received: 28.12.2017 • **Accepted/Published Online:** 28.11.2018 • **Final Version:** 15.01.2019

Abstract: In the Tavşanlı Zone, the Eocene magmatism led to NW-SE trending plutons located just south of the İzmir-Ankara-Erzincan Suture Zone in Turkey. The Middle Eocene-aged Günyüzü Intrusive Complex (Karacaören, Tekören, Dinek, Kadıncık) is one of these plutonic rocks and has metaluminous to peraluminous, medium-K calc-alkaline to shoshonitic and mainly I-type granite characteristics. The plutonic rocks consist of mainly granodiorite and granite, and their mafic microgranular enclaves are widespread in these rocks. Mineral assemblages in the host rocks and enclaves also are quite similar (quartz, plagioclase, K-feldspar, biotite, and hornblende), but the latter are more enriched in mafic minerals. The enclaves have disequilibrium textures such as oscillatory zoning and resorbed rims, indicating magma mixing/mingling. In the chondrite-normalized REEs patterns of the plutonic rocks are moderately fractionated and have small negative Eu anomalies. They are enriched in LILEs and LREEs relative to HFSEs, showing characteristics of subduction-related granitoids. The enclaves also have similar geochemical characteristics, indicating equilibration between the mafic and felsic magmas. Whole-rock geochemical data show that the parental magmas in the Günyüzü area were produced by partial melting from mafic crustal rocks and also magma mixing/mingling from enriched lithospheric mantle. Slab break-off is the likely mechanism for the initiation of the postcollisional magmatism in the Tavşanlı Zone.

Key words: Tavşanlı zone, granite, granodiorite, metaluminous, peraluminous, I-type, Rb-Sr geochronology

1. Introduction

The Anatolian plate is made up of various continental fragments and suture zones among them. These continental fragments are, from N to S, the Strandja Massif, the İstanbul and Sakarya Zones, the Anatolide-Tauride Block (Anatolide-Tauride Platform), the Central Anatolian Crystalline Complex (Kırşehir Massif, Kırşehir Block, Central Anatolian Massif), and the Arabian Platform (Şengör and Yılmaz, 1981; Şengör et al., 1982; Okay and Tüysüz, 1999) (Figure 1). The northwestern-western part of the Anatolide-Tauride Block consists of the Tavşanlı Zone, the Afyon Zone, and the Menderes Massif (Figure 1).

The Tavşanlı Zone is a ~250 km long and ~50 km wide east-west trending belt located just south of the İzmir-Ankara-Erzincan Suture Zone (Figures 1 and 2) (Okay, 2008). This suture zone represents the northern Neo-Tethyan ocean, which began to open between Laurasia and Gondwana from the Middle-Late Triassic (Tekin et al., 2002) and started to close between the Sakarya Zone and the Anatolide-Tauride Block during the Late Cretaceous (in the west) (e.g., Tüysüz et al., 1995; Meijers et al., 2010; Lefebvre et al., 2013). Following the collision, convergence between the Sakarya Zone and the Anatolide-Tauride Block remained until the Late Tertiary (Şengör and Yılmaz, 1981).

The zone is made up of blueschists tectonically overlain by an accretionary or mélange complex, peridotite slabs (Figure 2), and granodiorites (Okay et al., 1998). The blueschist sequence contains Permo-Triassic metapelitic schists at the base, overlain by Mesozoic marbles and a series of metabasite, metachert, and phyllite at the top (Okay, 1984). Metamorphic ages for the blueschists yield values between 80.1 ± 1.6 and 87.9 ± 0.3 Ma (Sherlock et al., 1999; Seaton et al., 2009). The Cretaceous accretionary or mélange complex consists of basalt, radiolarian chert, and pelagic shale, showing a low-grade incipient blueschist metamorphism (Okay, 2008). The Late Cretaceous (Dilek et al., 1999; Önen, 2003) large ophiolitic slabs contain

* Correspondence: mbagci@aku.edu.tr

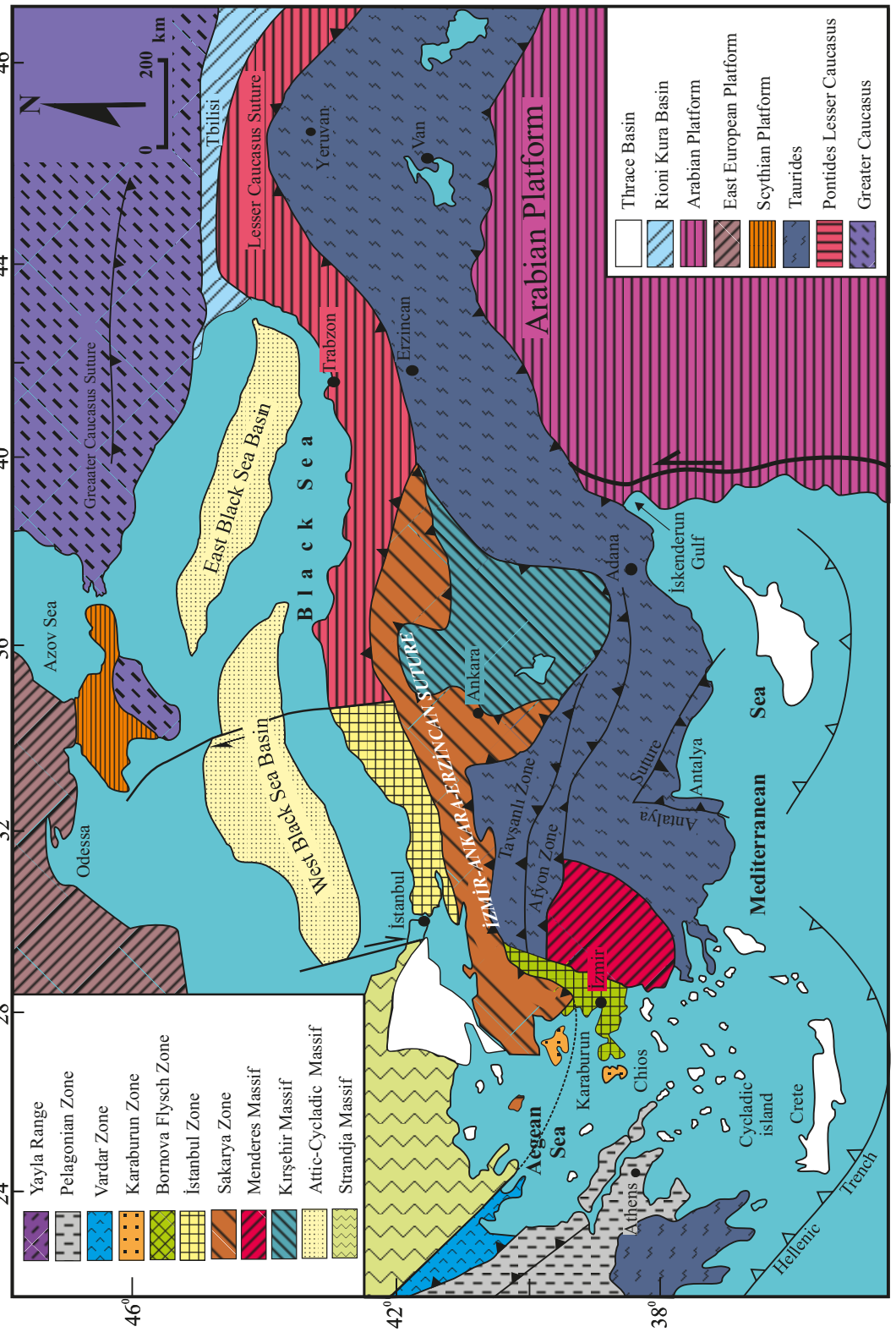

Figure 1. Tectonic map of the northeastern Mediterranean region showing the major sutures and continental blocks (after Okay and Tüysüz, 1999). Heavy lines with filled triangles show suture zones. Heavy lines with open triangles indicate active subduction zones.

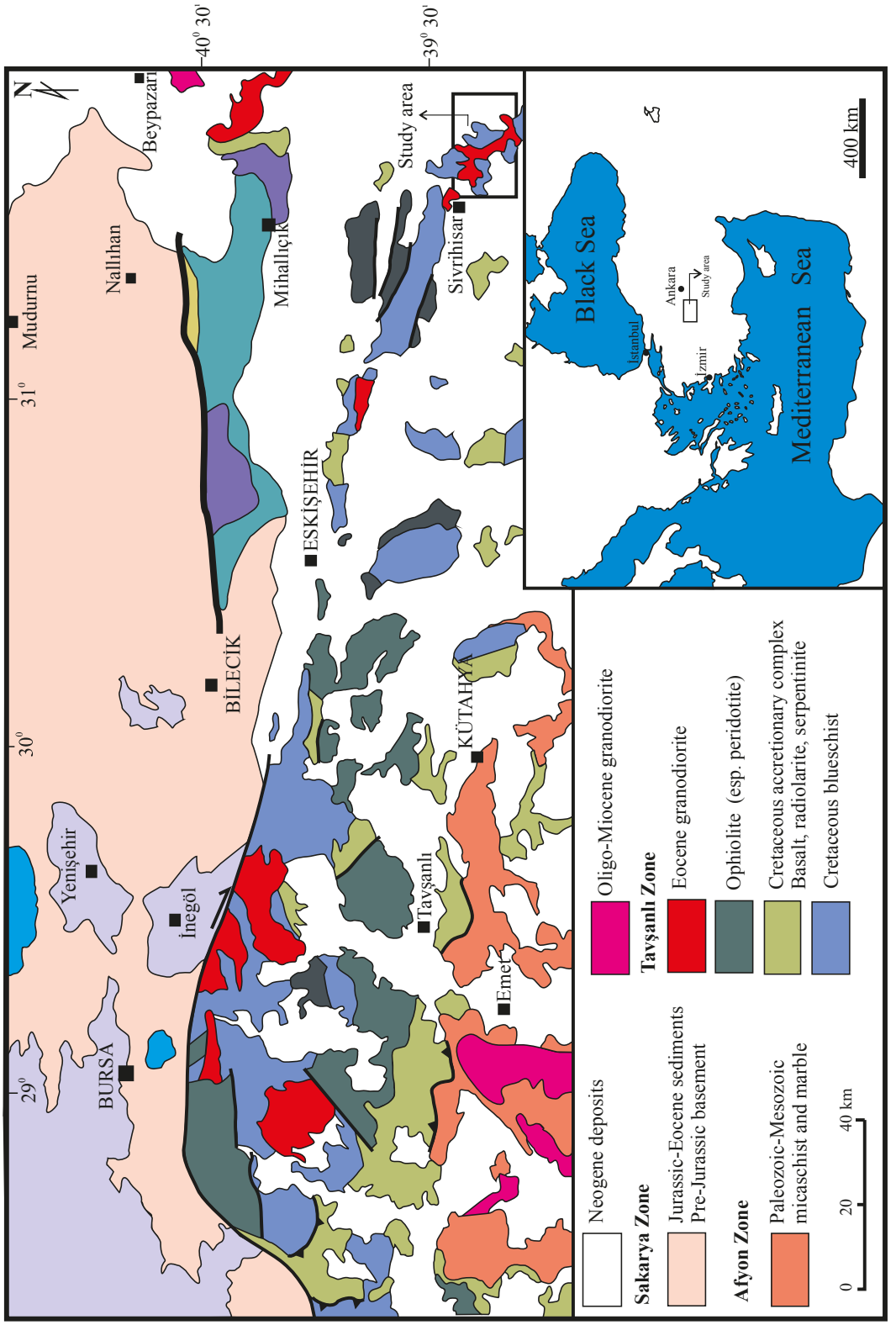

Figure 2. Geological map of the Tavşanlı Zone (after Okay, 2002).

mainly serpentinized harzburgite and dunite, and lesser pyroxenites, chromitites, and diabase dykes and rare gabbros (Lisenbee, 1972; Önen, 2003). The blueschists, an accretionary complex, and peridotite slabs in the zone are intruded by Eocene-aged plutonic rocks (e.g., Harris et al., 1994; Okay and Satır, 2006; Demirbilek, 2012; Demirbilek et al., 2018).

In this paper, we present a set of new geochronological and whole-rock geochemical data for the Günyüzü Intrusive Complex (GIC) in the Tavşanlı Zone in order to determine the emplacement ages of these rocks and reveal their magma sources and petrogenetic processes.

2. Local geological setting

The basement rocks of the Tavşanlı Zone are Paleozoic-aged metamorphic rocks (Figures 3 and 4). These rocks are composed mainly of gneiss, garnetschist, biotiteschist, quartzschist, calcschist, and marble (Demirbilek, 2012). According to Kibici et al. (1993) these rocks have undergone a regional greenschist facies metamorphism. Bağcı et al. (2011) divided these rocks into three zones on the basis of their metamorphism degree: in the core the rocks are gneissic in composition towards the upper series where they are garnetschist, biotiteschist, and quartzschist in composition, and in the uppermost series they are mainly marble and occasionally dolomitic in composition. These basement rocks are cut by the Cenozoic-aged GIC (Figures 3 and 4). The metamorphic and plutonic rocks are unconformably covered by the Pliocene-aged Günyüzü formation (Kibici et al., 1993). The rocks were deposited in a lacustrine environment and their compositions from older to younger are conglomerate, marl-claystone-gypsum-limestone, and limestone-marl-claystone (Kibici et al., 1993). Quaternary alluvium overlies all these rocks.

2.1. Field relations and petrology of the Günyüzü Intrusive Complex (GIC)

The GIC is a NW-SE-trending plutons covering about 50 km^2 (Figure 3). The contacts between intrusive complex and surrounding rocks are marked by the aplites and pegmatites.

On the basis of their textures and modal mineralogy, four subunits were recognized in the GIC (Kibici, 1994): gray, medium-grained Kadıncık granite (Figure 5a); gray, porphyritic with euhedral, zoned K-feldspar Dinek granite porphyry (Figure 5b); gray, medium-grained Tekören granite; and gray, fine- to medium-grained Karacaören granite (Kibici et al., 2008; İlbeyli and Kibici, 2009; Demirbilek, 2012; Demirbilek et al., 2018).

Contacts between these rocks types are usually gradational (Kibici, 1994; Kibici et al., 2008; İlbeyli and Kibici, 2009). The aplitic, pegmatitic and mafic dikes are widespread in the intrusive complex (Figure 5c). The aplitic and pegmatitic dykes are more common in the Kadıncık granite and Dinek granite porphyry compared to the Tekören and Karacaören granites. The pegmatitic dykes reach thickness up to tens of centimeters and lengths of up to tens of meters with mineral assemblage K-feldspar + plagioclase + quartz + muscovite ± biotite. Weathering is quite common in the Dinek granite porphyry and thus these rock types exhibit arenitization.

The GIC contains mafic microgranular enclaves (MMEs) showing both sharp and gradational contacts with the host rocks, locally having chilled margins or thin biotite-rich reaction rims (Figure 5d). The MMEs are ellipsoidal to lenticular and occasionally elongated in shape (Figure 5d). The MMEs are finer-grained compared to their host rocks. The MMEs are darker and more enriched in mafic minerals compared to the host rocks. They range in size from <1 cm to >1 m in diameter.

The intrusive complex is made up of mainly granodiorite and granite. The major constituent minerals are subhedral, oscillatory-zoned plagioclase (i.e. oligoclase-albite); subhedral, perthitic, simple, or cross-hatched twinned K-feldspar (i.e. orthoclase, microcline); and anhedral quartz, subhedral biotite, and subhedral hornblende (Figures 6a, 6b and 7a–7f). Accessory minerals are zircon, titanite, apatite, allanite, and opaque minerals. Alteration minerals include chlorite, epidote, sericite, and carbonate (Figures 6a, 6b, and 7a–7f).

The MMEs are mainly monzodiorite/monzogabbro in composition. They are hypidiomorphic-granular and range from fine- to medium-grained and porphyritic (Figures 6c and 6d). They are composed of the same minerals as their host rocks, namely plagioclase, K-feldspar, quartz, biotite, and amphibole. Accessory minerals include Fe-Ti oxides, titanite, zircon, and apatite. The enclaves contain more modal biotite and amphibole relative to the host granites. The MMEs also contain disequilibrium mixing textures (e.g., plagioclase: oscillatory zoning, patchy, rounded, and occasionally poikilitic rimmed by mafic minerals; biotite: blade-shaped; and apatite: needle-shaped) (Figure 6d).

3. Analytical techniques

All Rb-Sr analyses were performed on a GV IsoProbe T multicollector mass spectrometer at Geochron Laboratories, USA. Sr was loaded on Re filaments in a solution of $TaCl_5$ and H_3PO_4 and analyzed by dynamic multicollection. No fewer than 70 ratios were measured with a target intensity of ^{88}Sr = 3 V, providing a standard error for the mean of exponentially corrected $^{87}Sr/^{86}Sr$ of 0.0007%. Data were corrected for ^{87}Rb interference based on measured ^{85}Rb abundance, with fractionation corrected to $^{86}Sr/^{88}Sr$ = 0.1194, and reported with respect to a value

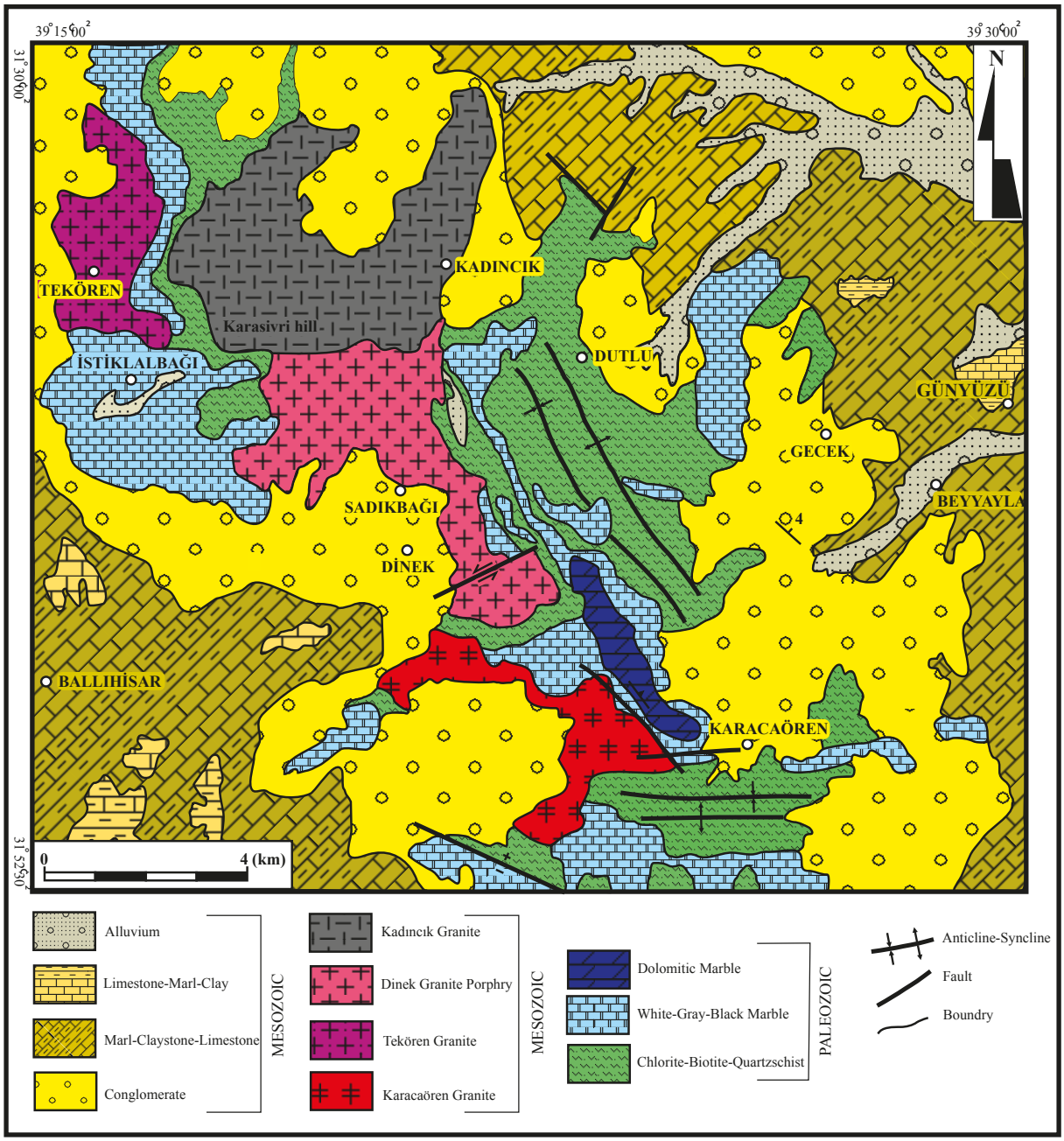

Figure 3. Geological map of the studied area (after Kibici et al., 1993).

of 0.710250 for NBS-987. The running mean of analyses of NBS-987 was 0.710242 ± 0.0000014 (n > 50), and no bias correction was made to the analytical data. The results are given in Table 1.

Thirty-one samples were analyzed for chemical analyses by X-ray fluorescence (XRF) using a Phillips 1400 wavelength dispersive spectrometer with excitation by a Rh-Xray tube at Acme Analytical Laboratories, Canada. Major oxides and minor element abundances from thirty-one samples were determined using ICP-MS following a $LiBO_2$ fusion and dilute nitric acid digestion. Loss on ignition (LOI) was determined by weight difference after ignition at 1000 °C. REE contents of the samples were measured by ICP-MS at Acme Analytical Laboratories, Canada. Representative chemical analyses of the intrusive complex are listed in Table 2.

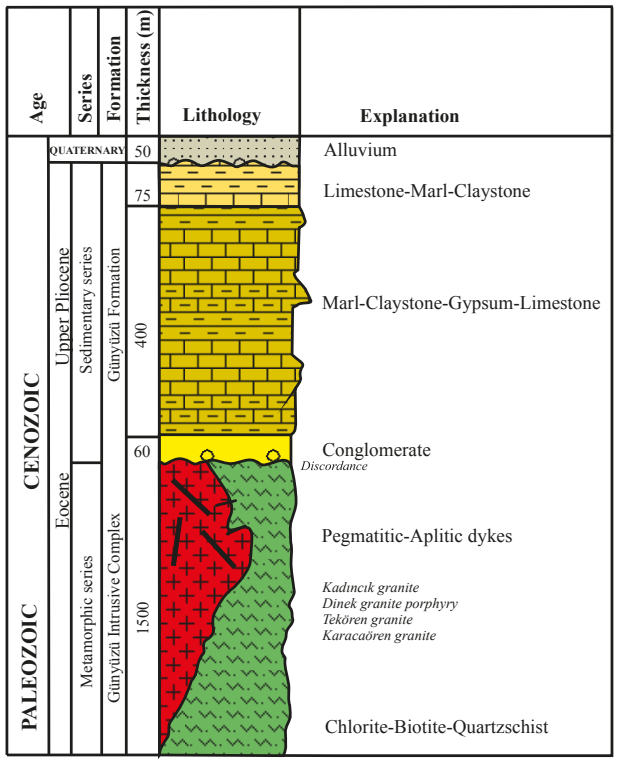

Figure 4. Generalized stratigraphic column of the studied area (after Kibici et al., 1993).

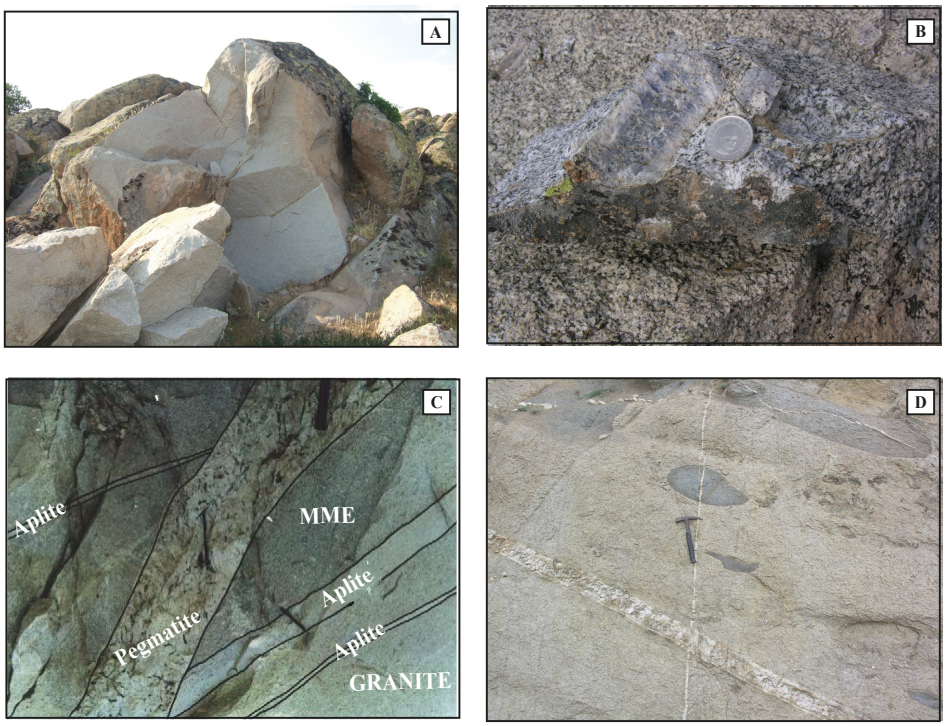

Figure 5. (a) An outcrop view of the Günyüzü Intrusive Complex (GIC); (b) close-up view of euhedral, zoned K-feldspar megacrysts in Dinek granite porphyry; (c) close-up view of aplitic and pegmatitic dykes cutting the host rock and the enclaves; and (d) field photograph of the GIC rocks and their enclaves. MME: Mafic microgranular enclave.

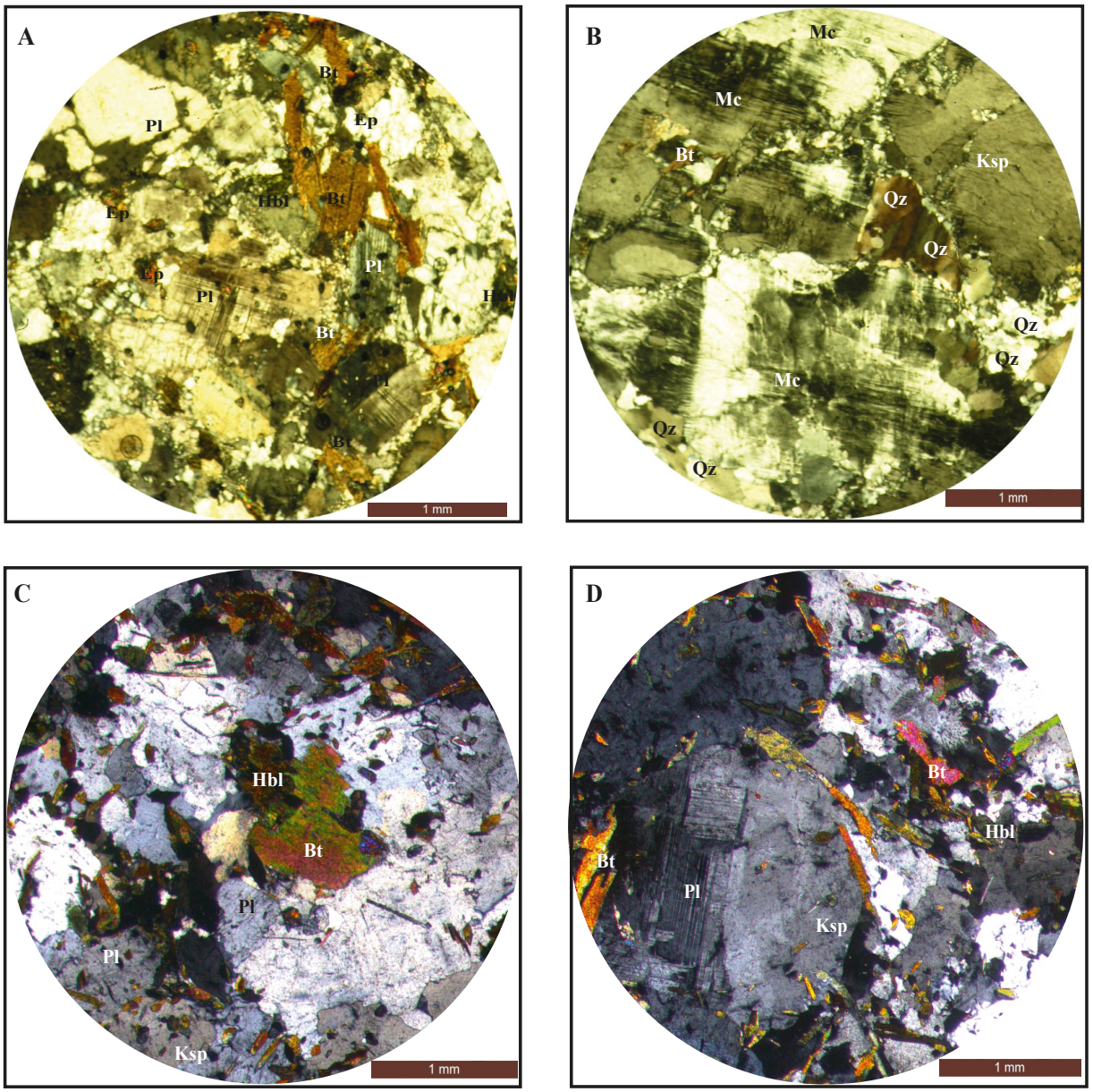

Figure 6. (a, b) Microscope photos of the granites (KGD-1, KGD-2; crossed polarized light, 5×) and (c, d) microscope photos of the MMEs (KANK1, KANK2; crossed polarized light, 5×). Bt: Biotite, Hbl: hornblende, Ksp: potassium feldspar, Mc: microcline, Pl: plagioclase, Qz: quartz.

4. Age of granite emplacement

The crystallization/emplacement ages for the plutonic rocks in the Tavşanlı Zone (Table 3) are still debated. Therefore, in this study, two different Günyüzü intrusive samples (three points from each sample) have been dated by the Rb-Sr method on whole rock. The isotopic compositions of the samples are presented in Table 1 and Rb-Sr whole-rock isochron ages of the Karacaören and Kadıncık samples are given in Figure 8. The plots of $^{87}Rb/^{86}Sr$ and $^{87}Sr/^{86}Sr$ ratios of the Kadıncık granite (Figure 8a) define an isochron corresponding to 40.8 ± 3.0 Ma (2s) with an initial $^{87}Sr/^{86}Sr$ ratio (Sr_i) of 0.7062 ± 0.0028 (2s), whereas those from the Karacaören granite (Figure 8b) yield an isochron age of 47.0 ± 1.0 Ma and slightly high initial Sr_i ratio of 0.70667 ± 0.00005. The mean square weighted deviates (MSWDs) are 0.012 and 0.18, respectively, for these granites. The whole-rock Rb-Sr isochron (Figure 8) ages for the GIC (Karacaören and Kadıncık samples) represent the time of emplacement of (Middle Eocene) plutons in the Tavşanlı Zone. Rb-Sr age

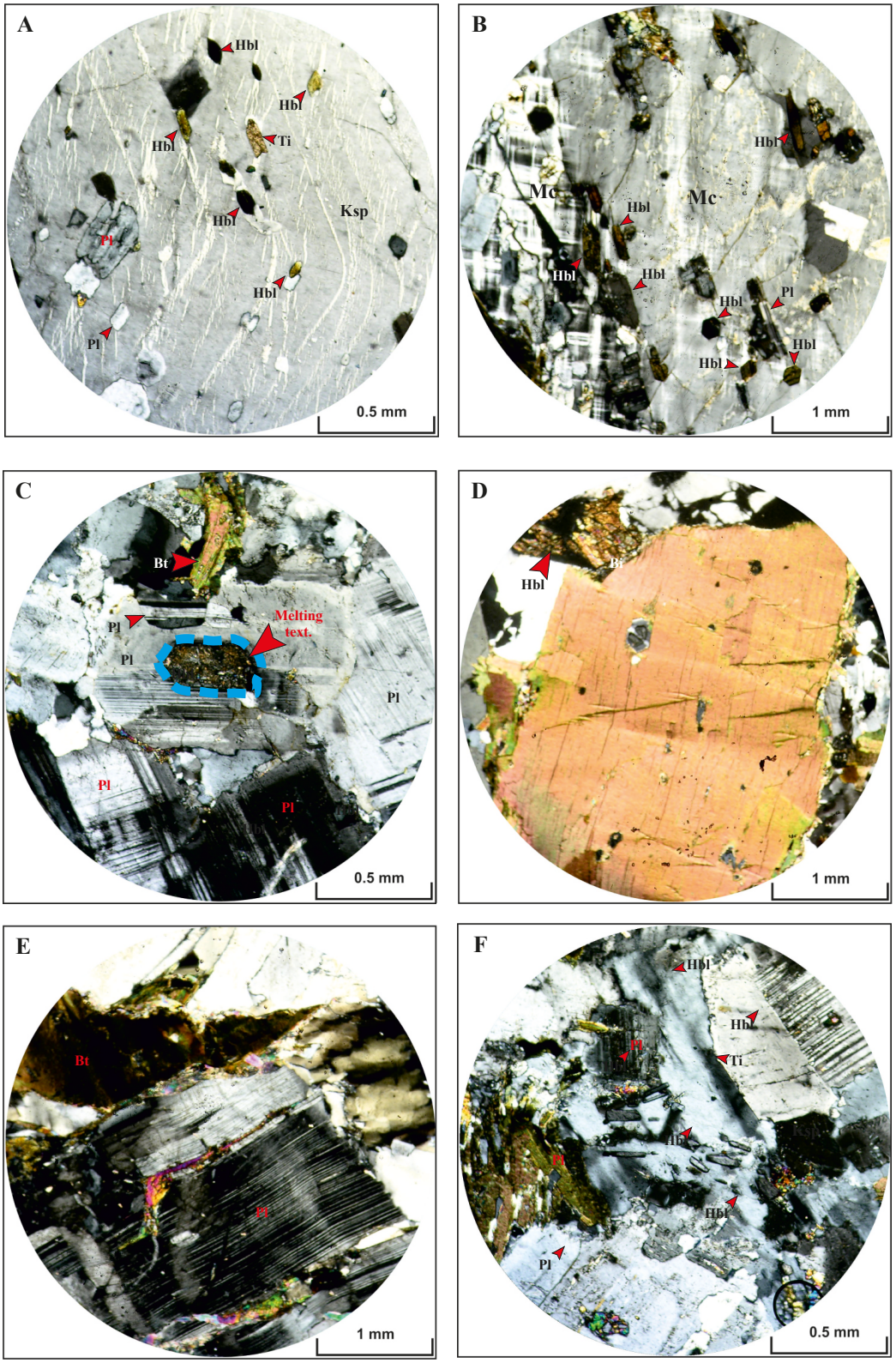

Figure 7. (a) Microscope photos of the granites; growth zones in K-feldspar grain from the Dinek granite porphyry (from Demirbilek, 2012); (b) mineral inclusions in microcline having poikilitic texture); (c) melting texture in some plagioclase minerals; and (d–f) subsolidus/deformation texture in biotite and plagioclase minerals reminiscent of kink-bands. Bt: Biotite, Hbl: hornblende, Ksp: potassium feldspar, Mc: microcline, Pl: plagioclase, Qz: quartz.

Table 1. Rb-Sr isotopic compositions of the Günyüzü Intrusive Complex (GIC).

Sample no.	Location	Rock type	SiO_2 (wt.%)	Rb (ppm)	Sr (ppm)	$^{87}Rb/^{86}Sr$	$^{87}Sr/^{86}Sr$	2s	$(^{87}Sr/^{86}Sr)_i$
Kgd-2	Kadıncık	Granite	69.23	725.4	21.11	101.22	0.77634	0.000017	0.70667
Kgd-2a	Kadıncık	Granite	69.23	16.82	88.19	0.5523	0.70703	0.000008	0.70665
Kgd-2b	Kadıncık	Granite	69.23	243.5	865.9	0.8137	0.70724	0.00001	0.70666
Kgr-6	Karacaören	Granodiorite	69.92	469.3	7.767	179.13	0.81000	0.000013	0.70620
Kgr-6a	Karacaören	Granodiorite	69.92	284.4	132	6.2379	0.70993	0.000009	0.70630
Kgr-6b	Karacaören	Granodiorite	69.92	1002	178.2	0.01634	0.70601	0.000008	0.70620

determinations are broadly similar to the published ages dated in other studies (Gautier, 1984, Demirbilek, 2012; Shin et al., 2013; Demirbilek et al., 2018).

5. Whole-rock geochemistry

5.1. Major elements

In the GIC, SiO_2 has a wide range from 66 to 75 wt.% and those from the MMEs have a narrow range from 48 to 66 wt.% (Table 2; Figure 9a). On the TAS diagram, these rocks plot in the granodiorite and granite fields, whereas the MMEs mainly plot in the monzodiorite/monzogabbro fields (Figures 9a and 9b). The total alkali-silica diagram (Figure 9a) shows that the rocks belong to the subalkaline series whereas the MMEs belong to the alkaline series. The K_2O versus SiO_2 diagram (Figure 9c) displays that the samples plot from medium-K calc-alkaline to shoshonite fields; however, the MMEs mainly plot in the high-K calc-alkaline field.

They are metaluminous to peraluminous with A/CNK [A/CNK = molar Al_2O_3 / ($CaO + Na_2O + K_2O$)] values between 0.88 and 1.10 (Figure 9d). Thus, the Günyüzü samples have medium-K calc-alkaline to shoshonitic and mainly I-type granite characteristics (Chappell and White, 1974). These features are also supported by the CIPW values (Table 4). In Table 4, the Tekören, Dinek, and Kadıncık samples have normative diopside; on the other hand, most of the silicic Karacaören samples have normative corundum.

As shown in the major element plots, the plutonic rocks and MMEs form well-defined trends of decreasing TiO_2, Al_2O_3, Fe_2O_{3t}, MnO (not shown), MgO, and CaO, and scattered Na_2O with increasing SiO_2 (Figure 10). The enclaves have higher concentrations of TiO_2, Al_2O_3, Fe_2O_3, MnO (not shown), MgO, and CaO compared to the host rocks (Figure 10).

5.2. Trace elements

In the selected Harker trace element diagrams (Figure 11), the enclaves have higher concentrations of Rb, Sr, Y, Zr, Nb, and Ba relative to the host rocks. In these diagrams Rb and Ba slightly increase with silica, whereas Y and Nb are somewhat constant. Sr and Zr slightly decrease with silica.

The chondrite-normalized REE patterns (Figure 12a) show that the GIC rocks and enclaves are enriched in light rare earth elements (LREEs) [$(La/Yb)_N$ = 4.21–22.6] with negative Eu anomalies (Eu/Eu^* = 0.52–0.87), except for two Karacaören samples displaying positive Eu anomalies. In addition they have flat to heavy rare earth elements (HREEs) enriched patterns [$(Gd/Lu)_N$ = 1.0–12.7]. The chondrite-normalized REE patterns of the MMEs show enrichment of the LREEs and negative Eu anomalies, similar to those of host rocks (Figure 12a).

In the primitive mantle-normalized multiple trace elements variation diagram (Figure 12b), the GIC samples and MMEs are characterized by enrichment in large ion lithophile elements (LILEs) (i.e. Rb, Ba, Th, U) and depletion in high field strength elements (HFSEs) (i.e. Ta, Nb, Zr, Hf) and also negative anomalies in K, P, and Ti (Figure 12b).

The samples from the GIC (>5% of modal quartz) are plotted on the tectonic discrimination diagrams of Pearce et al. (1984) (Figure 13). In the Nb-Y diagram (Figure 13a), they fall into the VAG and syn-COLG fields. In the Rb-(Y+Nb) discrimination diagram (Figure 13b), most of the intrusive samples plot within the VAG field.

6. Discussion

6.1. Petrogenesis: magma source, partial melting, fractional crystallization, and magma mixing/mingling

The rocks from the GIC have metaluminous to peraluminous, medium- through high-K calc-alkaline to shoshonitic and I-type granite characteristics (Figure 9). They are enriched in LILEs and depleted in HFSEs, displaying features of subduction-related rocks (Figure 12), which are also supported by the tectonic discrimination diagrams (Figure 13). Source rocks of subduction-related, high-K calc-alkaline magmatism could reflect a combination of processes, such as melting of continental crust, fractional crystallization, and crustal assimilation and magma mixing/mingling.

Table 2. XRF-major element (wt.%), trace element (ppm), ICP-MS rare earth elements, and Hf, Ta, Pb, Th, and U (ppm) analyses of representative samples from the Günyüzü Intrusive Complex (GIC), enclave, and dyke.

Sample no.	KGR-1	KGR-2	KGR-3	KGR-4	KGR-5	KGR-6	KGR-7	KGR-8	KGR-9	KGR-10
Location	Karacaören									
Rock type	Granite	Granite	Granodiorite	Granodiorite	Granodiorite	Granodiorite	Granodiorite	Granodiorite	Granite	Granite
SiO_2	74.43	73.1	69.12	72.64	69.42	69.92	68.27	69.56	74.4	72.56
TiO_2	0.03	0.03	0.27	0.03	0.22	0.19	0.25	0.27	0.03	0.03
Al_2O_3	14.14	14.8	15.57	15.13	16.27	15.93	16	16.01	14.09	14.75
Fe_2O_{3tot}	1.1	1.07	3.02	0.9	2.29	2.77	3.53	3.02	1.1	1.50
MnO	0.02	0.01	0.1	0.02	0.1	0.11	0.1	0.1	0.02	0.02
MgO	0.09	0.05	0.71	0.08	0.64	0.56	0.69	0.62	0.08	0.08
CaO	1.3	1.26	3.23	1.74	4.08	3.74	3.48	3.01	1.29	1.70
Na_2O	4.13	3.66	4.11	4.18	4.1	4.12	4.2	4.34	3.76	4.32
K_2O	3.86	4.89	2.45	4.33	1.38	1.54	2.47	1.87	4.42	3.57
P_2O_5	0.04	0.05	0.09	0.03	0.07	0.08	0.1	0.11	0.03	0.04
L.O.I.	0.7	0.9	1.1	0.7	1.3	0.9	0.7	0.9	0.6	1.20
TOTAL	99.82	99.83	99.78	99.76	99.84	99.86	99.79	99.8	99.79	99.78
Rb	109.9	126.9	77.1	134	43	47.8	80.9	85.5	124	105.00
Sr	135.6	135.7	429.7	185.6	416.3	392.4	476.6	405.5	150.9	169.00
Ba	1107	1128	735	1723	387	354	666	548	1447	1578.00
Zr	26.9	26.9	156.4	28.1	118.4	124.5	162.7	160.9	22.9	37.70
Hf	1.5	1.3	4.3	1.2	3.4	3.7	4.6	4.3	1	1.50
Ta	0.6	0.6	0.6	0.4	0.3	0.4	0.6	0.5	0.6	0.70
Th	3.4	5	14.8	6.5	8	5.6	19.9	18.1	3	3.00
U	0.6	5.9	2.6	0.8	1.2	1.4	2.9	2.7	0.6	1.00
Nb	7.6	8	9.5	6.3	6.2	5.7	8.7	9.1	4	7.40
Y	11.4	16.3	19.3	8.3	15.6	13.7	17.7	16.1	8	8.40
Cu	4.4	12.7	4.4	1.9	1.9	2.9	5.3	1.9	2.5	4.10
Zn	9	6	44	4	44	41	45	45	6	6.00
Pb	7.3	7.3	2	5.6	1.1	2.1	3.3	3.4	4.8	8.00
Cs	1.2	1	1.5	1.2	0.8	1	1.2	4.5	1.4	1.00
Ga	13.4	14.2	15.2	15.7	16.1	15.8	17.5	17.2	13.8	16.10
V	8	8	36	8	17	20	38	32	9	8.00
Ni	3.9	3.2	1.8	1.8	1.9	4.1	6.9	3.2	1.3	9.30
Co	0.6	0.8	3	0.4	2.2	2.2	3.2	2.5	0.5	0.70
Sc	2	1	4	2	3	3	3	4	2	2.00
La	6.2	10	33.1	14.3	29	14.7	36.8	34.5	4.8	4.80
Ce	12.9	17.7	64.9	28.5	59	29.7	71.2	66.2	8.8	9.50
Pr	1.41	2.28	6.69	3.13	6.2	3.23	7.17	6.68	0.97	1.00
Nd	5.2	8.3	22.7	11.6	21.5	11.8	24.1	22.5	3.7	3.90
Sm	1.31	2.02	3.91	2.28	3.59	2.16	3.84	3.61	1.02	1.00
Eu	0.42	0.5	0.92	0.59	0.92	0.72	0.91	0.88	0.49	0.52
Gd	1.31	1.95	3.11	1.78	2.7	1.82	2.84	2.61	0.96	1.04
Tb	0.27	0.38	0.54	0.27	0.44	0.32	0.49	0.45	0.21	0.20
Dy	1.71	2.41	2.97	1.42	2.64	1.87	2.98	2.73	1.26	1.33
Ho	0.37	0.51	0.63	0.28	0.49	0.41	0.6	0.55	0.25	0.26
Er	1.11	1.79	1.94	0.78	1.57	1.36	1.87	1.8	0.79	0.82
Tm	0.18	0.28	0.32	0.13	0.27	0.25	0.3	0.27	0.12	0.15
Yb	1.2	1.8	2.12	0.84	1.72	1.78	1.97	1.93	0.87	0.96
Lu	0.19	0.29	0.36	0.14	0.29	0.32	0.35	0.33	0.14	0.16
ΣREE	33.78	50.21	144.21	66.04	130.33	70.44	155.42	145.04	24.38	25.64
(La/Yb)n	3.71	3.98	11.20	12.21	12.09	5.92	13.40	12.82	3.96	3.59
(La/Sm)n	3.06	3.20	5.47	4.05	5.21	4.39	6.19	6.17	3.04	3.10
(Gd/Yb)n	9.03	8.96	12.14	17.53	12.99	8.46	11.93	11.19	9.13	8.96
Eu/Eu*	0.97	0.76	0.78	0.86	0.87	1.08	0.81	0.84	1.49	1.55
Mg#	7.56	4.46	19.03	8.16	21.84	16.82	16.35	17.03	6.78	5.06
A/CNK	1.52	1.51	1.59	1.48	1.70	1.69	1.58	1.74	1.49	1.54
A/NK	1.77	1.73	2.37	1.78	2.97	2.81	2.40	2.58	1.72	1.87
A.I.	0.47	0.55	0.28	0.49	0.17	0.19	0.28	0.22	0.53	0.42

Table 2. (Continued).

Sample no.	KGR-11	KGR-12	KGR-13	KGR-14	KGR-15	KGR-16	KGR-5A	KGR-7A	KDG-1
Location	Karacaören								Kadıncık
Rock type	Granite	Granodiorite	Granodiorite	Granite	Granodiorite	Granodiorite	Granodiorite	Granodiorite	Granodiorite
SiO_2	73.68	68.65	70.61	75.16	68.69	69.37	68.89	67.14	65.62
TiO_2	0.04	0.28	0.24	0.03	0.26	0.23	0.24	0.27	0.34
Al_2O_3	14.66	16.25	15.46	13.99	15.92	15.61	16.46	16.35	17.13
Fe_2O_3tot	0.91	3.26	2.93	0.88	3.58	3.05	2.43	3.05	3.07
MnO	0.02	0.07	0.08	0.02	0.10	0.09	0.11	0.10	0.08
MgO	0.09	0.55	0.57	0.08	0.64	0.54	0.65	0.73	1.09
CaO	0.45	3.18	2.77	0.60	3.50	3.16	3.68	3.61	4.19
Na_2O	3.91	4.34	4.11	4.05	4.11	4.19	4.00	4.26	5.05
K_2O	5.13	1.22	1.18	4.42	1.71	2.21	1.43	2.12	2.12
P_2O_5	0.04	0.11	0.08	0.04	0.11	0.10	0.06	0.11	0.17
L.O.I.	0.90	1.90	1.80	0.60	1.20	1.30	1.90	2.00	0.80
TOTAL	99.82	99.83	99.83	99.83	99.79	99.81	99.82	99.78	99.67
Rb	163.50	59.90	82.80	141.60	58.50	66.50	43.10	66.50	61.30
Sr	97.30	400.10	351.50	87.80	453.80	413.40	389.30	470.90	1067.20
Ba	1156.00	276.00	510.00	966.00	616.00	561.00	562.00	590.00	906.00
Zr	30.40	188.00	155.10	43.60	168.40	142.50	118.60	172.20	190.30
Hf	1.40	5.30	4.00	1.60	4.60	3.90	3.10	4.40	5.60
Ta	1.20	0.70	0.40	1.20	0.60	0.50	0.50	0.70	0.60
Th	4.90	16.90	11.70	6.20	16.90	17.20	9.20	19.00	16.30
U	1.50	1.80	1.90	1.40	2.40	1.70	1.20	2.60	3.10
Nb	15.40	11.90	10.40	9.70	8.90	8.60	6.10	9.50	9.70
Y	16.00	22.20	15.80	20.60	19.20	16.10	15.50	18.30	17.60
Cu	1.20	2.60	3.30	1.30	3.40	2.80	2.60	5.20	7.20
Zn	2.00	39.00	38.00	2.00	47.00	42.00	54.00	47.00	50.00
Pb	8.40	2.90	3.70	9.60	2.40	2.60	2.00	3.20	3.50
Cs	1.90	2.90	4.70	1.90	1.80	0.90	1.00	0.90	3.30
Ga	14.40	17.60	16.10	14.00	17.00	15.70	16.20	16.40	19.80
V	8.00	32.00	26.00	8.00	33.00	28.00	19.00	32.00	52.00
Ni	2.60	4.70	4.50	2.30	7.60	5.10	4.60	3.30	3.80
Co	0.40	2.30	2.30	0.50	2.90	2.70	2.20	2.60	4.90
Sc	4.00	4.00	5.00	3.00	4.00	3.00	4.00	4.00	5.00
La	8.90	32.20	25.60	8.30	37.30	42.70	30.80	36.80	43.90
Ce	19.70	59.50	55.30	16.90	71.40	84.10	65.90	74.60	87.00
Pr	2.44	6.58	5.39	1.98	7.16	7.72	6.51	7.05	9.15
Nd	9.10	22.90	18.00	7.50	25.90	26.90	23.00	25.80	33.60
Sm	2.82	4.35	3.54	2.13	4.13	3.81	3.66	4.21	5.32
Eu	0.44	1.05	0.87	0.38	0.99	0.92	0.92	0.97	1.35
Gd	2.83	3.42	3.00	2.54	3.25	2.80	2.78	3.34	3.90
Tb	0.52	0.60	0.53	0.52	0.56	0.49	0.46	0.54	0.58
Dy	2.99	3.49	3.22	3.38	3.21	2.63	2.41	3.04	2.88
Ho	0.50	0.72	0.56	0.64	0.71	0.58	0.52	0.63	0.55
Er	1.56	2.28	1.75	1.93	2.07	1.80	1.64	2.08	1.56
Tm	0.23	0.35	0.29	0.31	0.35	0.30	0.27	0.34	0.24
Yb	1.55	2.53	1.87	1.97	2.36	2.09	1.95	2.32	1.72
Lu	0.24	0.42	0.30	0.32	0.39	0.35	0.33	0.36	0.26
ΣREE	53.82	140.39	120.22	48.80	159.78	177.19	141.15	162.08	192.01
(La/Yb)n	4.12	9.13	9.82	3.02	11.34	14.65	11.33	11.38	18.31
(La/Sm)n	2.04	4.78	4.67	2.52	5.83	7.24	5.43	5.64	5.33
(Gd/Yb)n	15.10	11.18	13.27	10.67	11.39	11.08	11.79	11.91	18.76
Eu/Eu*	0.47	0.80	0.80	0.50	0.80	0.82	0.85	0.76	0.87
Mg#	9.00	14.44	16.29	8.33	15.17	15.04	21.10	19.31	26.20
A/CNK	1.54	1.86	1.92	1.54	1.71	1.63	1.81	1.64	1.51
A/NK	1.62	2.92	2.92	1.65	2.74	2.44	3.03	2.56	2.39
A.I.	0.59	0.16	0.16	0.54	0.20	0.26	0.17	0.24	0.24

Table 2. (Continued).

Sample no.	KDG-2	GRP-1	GRP-2	TEK-1	TEK-2	KANK-1	KGR-DY	DIY-1	DIY-2	DY-3	KGD-AP-1
Location	Kadıncık	Dinek		Tekören		Enclaves from the Günyüzü Intrusive Complex					Kadıncık
Rock type	Granodiorite	Quartz-monzonite	Quartz-monzonite	Granodiorite	Granodiorite	Enclave	Enclave	Enclave	Enclave	Enclave	Aplitic dyke
SiO_2	69.23	66.35	66.71	63.19	66.26	55.61	52.61	51.24	47.94	56.36	74.94
TiO_2	0.25	0.23	0.26	0.40	0.28	0.58	1.06	1.08	0.96	1.03	0.06
Al_2O_3	15.45	16.87	16.71	16.73	16.39	14.49	16.38	16.10	18.53	18.83	14.18
Fe_2O_{3tot}	2.78	2.22	2.60	4.16	3.22	11.53	7.20	7.45	8.09	5.60	0.91
MnO	0.07	0.05	0.06	0.08	0.07	0.37	0.13	0.14	0.13	0.10	0.08
MgO	0.80	0.93	0.97	1.93	1.27	4.22	5.71	6.35	4.92	2.12	0.13
CaO	3.16	2.79	3.41	4.77	3.54	6.41	6.29	6.91	8.35	1.36	0.95
Na_2O	4.61	4.45	5.22	4.74	4.33	3.77	4.63	4.50	3.68	2.72	3.73
K_2O	2.53	5.11	2.86	2.22	3.14	1.66	1.90	1.62	1.22	2.37	4.02
P_2O_5	0.11	0.11	0.11	0.23	0.19	0.15	0.25	0.23	0.20	0.27	0.01
L.O.I.	0.70	0.50	0.80	1.20	1.00	0.90	3.50	4.00	5.70	9.00	0.80
TOTAL	99.70	99.60	99.72	99.66	99.69	99.71	99.72	99.70	99.75	99.81	99.82
Rb	75.60	160.80	102.10	60.30	76.50	60.90	38.60	32.70	37.00	76.70	137.90
Sr	881.90	1000.70	981.80	1018.20	941.20	558.90	484.90	488.70	419.40	166.70	199.40
Ba	986.00	1783.00	705.00	896.00	988.00	342.00	375.00	438.00	262.00	263.00	1070.00
Zr	152.80	141.70	164.50	161.50	125.30	110.60	118.70	115.00	83.80	147.60	44.00
Hf	4.80	3.90	5.00	4.20	3.60	3.40	3.30	2.80	2.30	3.40	2.20
Ta	0.50	0.40	0.40	0.50	0.50	0.20	1.00	1.00	0.40	0.90	1.10
Th	12.60	14.20	14.50	16.50	11.00	5.70	4.50	3.80	3.50	5.90	6.80
U	5.20	4.50	3.40	2.00	1.70	3.60	2.10	1.70	1.30	2.40	3.10
Nb	8.70	7.30	8.30	9.90	6.90	9.90	15.60	15.40	7.70	16.60	12.00
Y	14.30	10.00	11.60	17.80	12.90	26.90	20.00	19.70	22.20	20.20	12.70
Cu	3.60	6.80	8.90	8.10	7.00	9.00	49.40	42.10	47.00	36.80	7.60
Zn	51.00	31.00	40.00	44.00	38.00	140.00	43.00	43.00	52.00	59.00	18.00
Pb	5.70	9.80	9.80	3.70	4.60	4.40	4.70	3.30	2.60	6.30	8.50
Cs	2.70	3.10	2.40	2.10	1.80	3.40	0.20	0.40	1.10	3.20	2.60
Ga	17.20	18.10	19.10	18.70	16.90	25.70	16.10	14.70	17.60	17.40	13.60
V	34.00	39.00	42.00	71.00	49.00	138.00	182.00	191.00	220.00	147.00	13.00
Ni	5.70	5.40	8.40	12.10	10.00	26.30	49.30	53.60	15.60	35.60	2.50
Co	3.60	4.30	5.40	8.80	6.40	14.70	23.00	25.80	22.50	15.50	0.50
Sc	4.00	4.00	4.00	9.00	6.00	26.00	25.00	27.00	25.00	16.00	3.00
La	33.80	30.90	35.90	50.10	32.40	17.10	15.40	14.70	11.30	17.70	8.00
Ce	68.10	61.10	72.40	100.70	66.30	33.70	34.00	33.10	23.50	44.00	15.40
Pr	7.04	6.56	7.51	10.61	7.02	3.71	3.82	3.67	2.88	4.22	2.00
Nd	25.50	24.80	27.70	38.90	26.00	14.10	16.00	15.30	12.90	17.30	8.10
Sm	3.95	3.63	4.11	6.12	4.26	3.50	3.30	3.39	3.04	3.46	2.07
Eu	0.96	0.97	1.05	1.52	1.10	0.99	1.05	1.09	1.02	0.97	0.51
Gd	2.92	2.59	2.82	4.24	3.12	3.82	3.56	3.53	3.49	3.36	1.97
Tb	0.43	0.35	0.38	0.59	0.45	0.67	0.57	0.59	0.59	0.58	0.38
Dy	2.45	1.76	1.90	2.92	2.25	3.96	3.20	3.54	3.30	3.32	2.25
Ho	0.46	0.31	0.36	0.55	0.43	0.83	0.69	0.68	0.73	0.73	0.45
Er	1.36	0.92	0.96	1.60	1.22	2.73	2.01	2.14	2.15	2.40	1.36
Tm	0.22	0.14	0.15	0.23	0.19	0.43	0.31	0.32	0.31	0.36	0.23
Yb	1.48	0.92	1.09	1.64	1.27	2.89	1.97	2.06	1.98	2.52	1.73
Lu	0.23	0.15	0.17	0.24	0.19	0.46	0.31	0.31	0.32	0.39	0.28
ΣREE	148.90	135.10	156.50	219.96	146.20	88.89	86.19	84.42	67.51	101.31	44.73
(La/Yb)n	16.38	24.09	23.62	21.91	18.30	4.24	5.61	5.12	4.09	5.04	3.32
(La/Sm)n	5.52	5.50	5.64	5.28	4.91	3.15	3.01	2.80	2.40	3.30	2.49
(Gd/Yb)n	16.32	23.29	21.40	21.39	20.32	10.93	14.95	14.18	14.58	11.03	9.42
Eu/Eu*	0.83	0.92	0.89	0.86	0.88	0.82	0.93	0.96	0.95	0.86	0.76
Mg#	22.35	29.52	27.17	31.69	28.29	26.79	44.23	46.01	37.82	27.46	12.50
A/CNK	1.50	1.37	1.45	1.43	1.49	1.22	1.28	1.24	1.40	2.92	1.63
A/NK	2.16	1.76	2.07	2.40	2.19	2.67	2.51	2.63	3.78	3.70	1.83
A.I.	0.30	0.51	0.31	0.25	0.34	0.22	0.22	0.20	0.13	0.22	0.48

Table 3. Age data for the Tavşanlı Zone plutonic rocks.

Pluton	Rock type	Method	Mineral	Sample num.	Age (Ma)	References
Yürükcaören	Granitoid	U-Pb	Zircon	-	66.93 ±4.84	Gautier (1984)
Topkaya	Granitoid	U-Pb	Zircon	-	65.91 ± 3.84	Gautier (1984)
Kaymaz	Granitoid	U-Pb	Zircon	-	84.98 ± 6.27	Gautier (1984)
	Granite	U-Pb	Zircon	-	33.3 ± 2.0 – 42.5 ± 2.2	Shin et al. (2013)
	Granite	K/Ar	Feldspar	Kyg-9	52.1 ± 2.0	Demirbilek (2012), Demirbilek et al. (2018)
	Granite	K/Ar	Feldspar	Kyg-9	54.0 ± 2.1	Demirbilek (2012), Demirbilek et al. (2018)
Sivrihisar	Monzonite	U-Pb	Zircon	-	90.82 ± 2.14	Gautier (1984)
		U-Pb	Apatite	-	48.95 ± 4.49	Gautier (1984)
	Granitoid	^{40}Ar-^{39}Ar	Hornblende	-	53.0 ± 3.0	Sherlock et al. (1999)
		K/Ar	Hornblende	-	71.0 ± 3.0	Çoğulu and Krummenacher (1967)
		K/Ar	Biotite	-	62.9 ± 1.3	Delaloye and Bingöl (2000)
		K/Ar	Feldspar	-	61.0 ± 1.4	Delaloye and Bingöl (2000)
		K/Ar	Hornblende	-	56.8 ± 1.2	Delaloye and Bingöl (2000)
	Monzonite-syenite	U-Pb	Zircon	-	42.4 ± 2.3 –78.4 ± 8.5	Shin et al. (2013)
	Quartz monzonite	K/Ar	Hornblende	Sgr-2	51.2 ± 2.3	Demirbilek (2012), Demirbilek et al. (2018)
	Quartz monzonite	K/Ar	Feldspar	Sgr-2	44.7 ± 1.7	Demirbilek (2012), Demirbilek et al. (2018)
	Quartz monzonite	K/Ar	Hornblende	Sgr-23	53.2 ± 2.1	Demirbilek (2012), Demirbilek et al. (2018)
	Quartz monzonite	K/Ar	Feldspar	Sgr-23	48.4 ± 1.9	Demirbilek (2012), Demirbilek et al. (2018)
Günyüzü						
Tekören	Granodiorite	K/Ar	Hornblende	Tgr-2a	57.8 ± 2.3	Demirbilek (2012), Demirbilek et al. (2018)
		K/Ar	Biotite	Tgr-2a	52.5 ± 2.0	Demirbilek (2012), Demirbilek et al. (2018)
		K/Ar	Feldspar	Tgr-2a	46.1 ± 1.8	Demirbilek (2012), Demirbilek et al. (2018)
Kadıncık	Granodiorite	K/Ar	Biotite	Kgd-20	52.1 ± 2.1	Demirbilek (2012), Demirbilek et al. (2018)
		K/Ar	Hornblende	Kgd-20	52.8 ± 2.4	Demirbilek (2012), Demirbilek et al. (2018)
		K/Ar	Feldspar	Kgd-20	50.5 ± 2.1	Demirbilek (2012), Demirbilek et al. (2018)
Dinek	Quartz monzodiorite	K/Ar	Hornblende	Grp-2a	55.9 ± 2.7	Demirbilek (2012), Demirbilek et al. (2018)
	Quartz monzodiorite	K/Ar	Biotite	Grp-2a	48.0 ± 1.9	Demirbilek (2012), Demirbilek et al. (2018)
	Quartz monzodiorite	K/Ar	Feldspar	Grp-2a	45.3 ± 1.8	Demirbilek (2012), Demirbilek et al. (2018)
Karacaören	Granodiorite	K/Ar	Hornblende	Kgr-10	59.3 ± 3.0	Demirbilek (2012), Demirbilek et al. (2018)
		K/Ar	Biotite	Kgr-10	47.6 ± 1.8	Demirbilek (2012), Demirbilek et al. (2018)
		K/Ar	Feldspar	Kgr-10	49.6 ± 1.9	Demirbilek (2012),Demirbilek et al. (2018)

The GIC samples increase in SiO_2, K_2O, and Rb and decrease in TiO_2, Al_2O_3, Fe_2O_{3t}, MgO, CaO, and P_2O_5 (not shown) contents, consistent with their evolution through fractional crystallization (Figures 10 and 11). In addition, the decrease of Al_2O_3, Fe_2O_{3t}, MgO, CaO, Sr, Eu/Eu*, and Dy/Yb with an increase in SiO_2 indicates plagioclase, K-feldspar, hornblende, and biotite fractionation during magma evolution (Figures 10b–10e, 11b, 14c, and 14d). Figures 14a and 14b also show plagioclase, K-feldspar, and biotite fractionations. Other minor minerals have

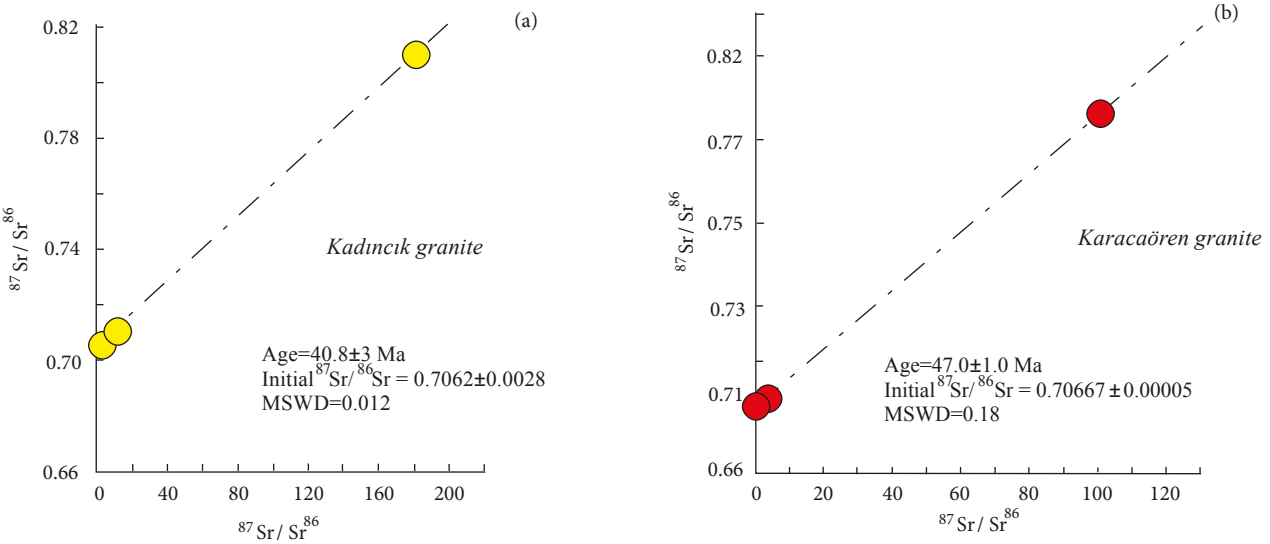

Figure 8. Rb-Sr whole-rock isochron for (a) the Kadıncık granite and (b) the Karacaören granite. The Isoplot program (Ludwig, 2003) was used for the data reduction and determination of statistical ages.

also been fractionated during magma crystallization, such as Fe-Ti oxides and apatite, as revealed by the negative correlations between SiO_2-TiO_2 (Figure 10a) and SiO_2-P_2O_5 (not shown). These correlations are also accompanied by negative Ti and P anomalies in the primitive mantle-normalized multielement diagram (Figure 12b). On the other hand, some geochemical characteristics for the GIC rocks cannot be solely interpreted by fractional crystallization. For example, the rocks have high K_2O and Rb compositions and also low contents of MgO, Sc, V, Ni, and Co (Table 2).

The medium- and high-K calc-alkaline to shoshonitic and I-type granodiorite and granite can also be formed from partial melting of crustal melts (e.g., Patīno Douce, 1996, 1999). The high ratios of CaO/Na_2O and $CaO/(MgO+FeO_t)$ but low ratios of Al_2O_3/TiO_2, $Al_2O_3/(MgO+FeO_t)$, Rb/Ba, and Rb/Sr (Figures 15a and 15b) indicate that the granodiorites and granites were derived from different sources (Demirbilek, 2012; Demirbilek and Mutlu, 2012; Demirbilek et al., 2018; this study).

CaO/Na_2O versus Al_2O_3/TiO_2 and Rb/Ba versus Rb/Sr (Figures 15a and 15b) of the plutonic rocks indicate that the least silicic Karacaören, Tekören, Dinek, and Kadıncık samples were derived from mafic melts whereas those from the most silicic Karacaören samples originated from crustal melts.

Compositional variations of these rocks can be caused by variable melting conditions (e.g., temperature, pressure, oxygen fugacity, and H_2O content) (e.g., Wolf and Wyllie, 1994; Gardien et al., 1995; Patīno Douce and Beard, 1995, 1996; Patīno Douce, 1996; Singh and Johannes, 1996; Thompson, 1996; Patīno Douce and McCarthy, 1998; Jung et al., 2000) or resulted from different source rocks, i.e. metapelites, metagraywackes, and amphibolites (e.g., Gardien et al., 1995; Thompson, 1996; Altherr et al., 2000; Wang et al., 2007; Karacık et al., 2008; Karacık and Tüysüz, 2010; Demirbilek, 2012; Demirbilek et al., 2018). Source variation can be also seen from Figure 15c, showing that the granodiorites were generated from partial melting of amphibolites, and the granites were derived from partial melting of felsic pelites.

The MMEs are common in the GIC, indicating mixing of crustal and mantle magmas. For example, the MMEs display chilled margins against the host rocks (Figures 5c and 5d), revealing they were originally magma globules that strained and quenched to finer-grained solid enclaves in the host magma (e.g., Reid et al., 1983; Vernon et al., 1988; Fernandez and Barbarin, 1991; Poli and Tommasini, 1991; Barbarin, 1992; Hibbard, 1995; Kumar and Rino, 2006; Perugini and Poli, 2012; Vernon, 2014). Some enclaves have fine-grained margins indicating that mafic magma cooled rapidly against host acidic magma (e.g., Didier, 1973; Vernon, 1983, 1984).

In addition to MMEs, K-feldspar megacrystals (Figures 5b, 7a, and 7b) in the GIC (esp. Dinek granite porphyr) could also indicate the importance of magma mixing/mingling process in the evolution of these rocks. K-feldspar is the mineral cooling in the last phases of the fractional crystallization. Because of this, it is not possible to see the development of euhedral K-feldspar megacrystals within the process of the magmatic solidification. It may be interpreted that the megacrysts in

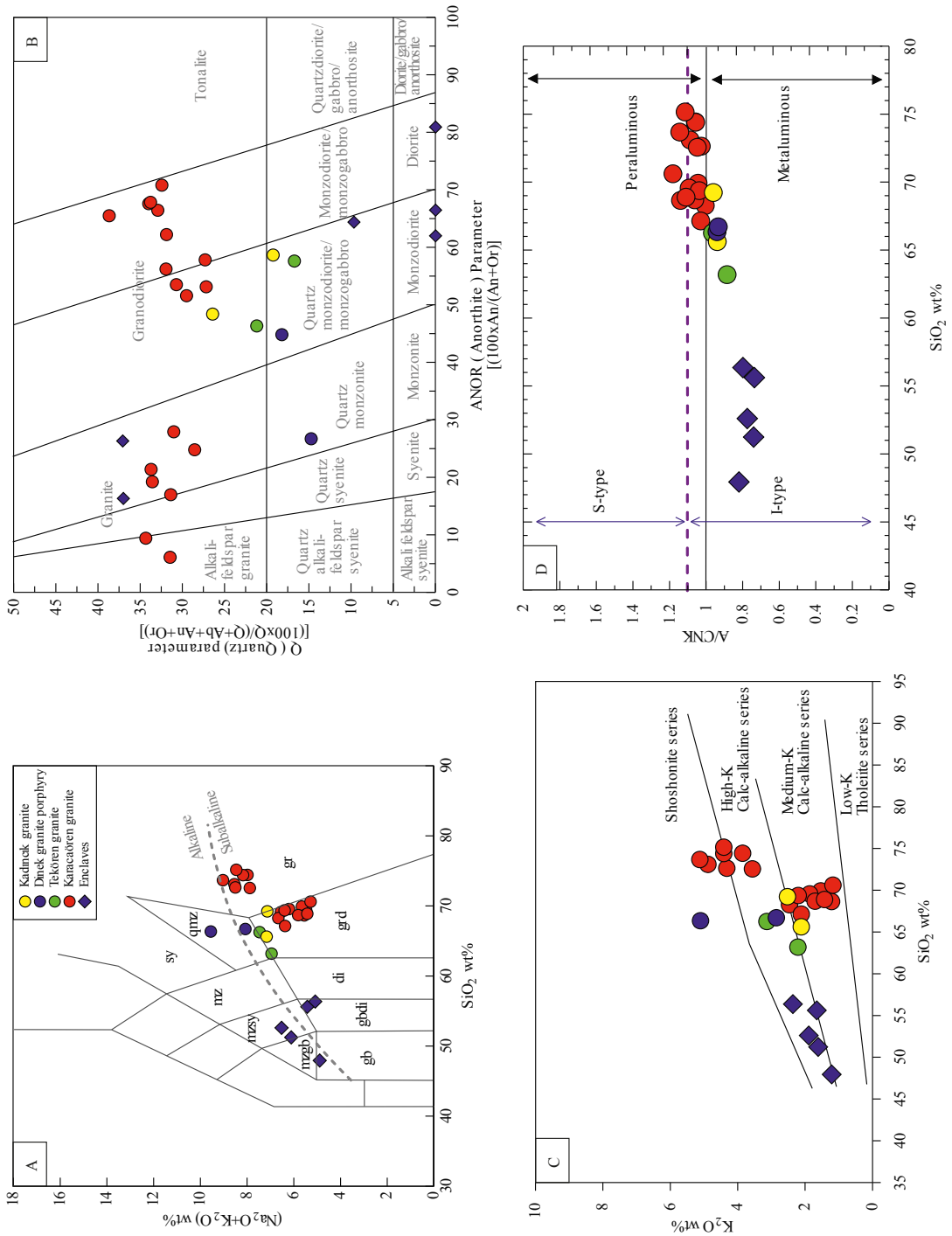

Figure 9. (a) Total alkali (Na_2O+K_2O) versus SiO_2 diagram of the Günyüzü Intrusive Complex (GIC) (after Middlemost, 1994); (b) CIPW normative compositions (Streckeisen and Le Maitre, 1979). mzgb: Monzogabbro, mzsy: monzosyenite, mz: monzonite, qmz: quartz monzonite, sy: syenite, gb: gabbro, gbdi: gabbroic diorite, di: diorite, grd: granodiorite, and gr: granite. Plot of Q parameter vs. ANOR parameter (after Streckeisen and Le Maitre, 1979) used to classify the Tavşanlı zone plutons [Q parameter = 100 × (Q + Or + Ab + An)]; [ANOR parameter = 100 × (Or + An)]; note: the norm calculations are made following the procedure outlined by Cox et al. (1979); (c) K_2O versus SiO_2 diagram (after Rickwood, 1989); and (d) A/CNK versus SiO_2 diagram of the GIC (after Clarke, 1992).

Table 4. CIPW normative mineralogy of the samples belonging to Günyüzü Intrusive Complex (GIC).

Sample no.	Location	Quartz	Anorthite	Diopside	Hypersthene	Albite	Orthoclase	Olivine	Apatite	Pyrite	Ilmenite	Corundum	Magnetite	TOTAL
KGR-1	Karacaören	32.46	6.19	-	0.71	34.86	22.75	-	0.09	0.42	0.06	0.88	1.59	100.00
KGR-2	Karacaören	30.13	5.92	-	0.97	30.97	28.96	-	0.12	-	0.06	1.32	1.55	100.00
KGR-3	Karacaören	26.72	15.24	-	3.94	34.27	14.30	-	0.21	-	0.51	0.49	4.32	100.00
KGR-4	Karacaören	27.74	8.44	-	0.93	35.37	25.59	-	0.07	-	0.06	0.49	1.30	99.99
KGR-5	Karacaören	29.86	19.63	-	3.30	34.44	8.10	-	0.16	-	0.42	0.80	3.31	100.00
KGR-6	Karacaören	30.01	17.78	-	3.52	34.35	8.98	-	0.19	-	0.36	0.86	3.96	100.00
KGR-7	Karacaören	24.38	16.21	-	4.32	34.78	14.30	-	0.23	-	0.46	0.33	5.00	100.00
KGR-8	Karacaören	28.63	13.97	-	3.71	36.13	10.87	-	0.25	-	0.51	1.62	4.31	100.00
KGR-9	Karacaören	32.34	6.20	-	1.10	31.73	26.06	-	0.07	-	0.06	0.84	1.59	100.00
KGR-10	Karacaören	29.62	8.17	-	1.43	36.55	21.10	-	0.09	-	0.06	0.79	2.17	99.99
KGR-11	Karacaören	30.08	1.97	-	0.95	33.17	30.38	-	0.09	-	0.08	1.97	1.32	100.00
KGR-12	Karacaören	30.11	14.91	-	3.71	36.39	7.15	-	0.25	-	0.53	2.26	4.68	100.00
KGR-13	Karacaören	34.43	13.12	-	3.58	34.52	6.91	-	0.19	-	0.46	2.57	4.22	100.00
KGR-14	Karacaören	33.02	2.72	-	0.91	34.27	26.12	-	0.09	-	0.06	1.54	1.28	100.00
KGR-15	Karacaören	28.31	16.35	-	4.22	34.19	9.93	-	0.25	-	0.49	1.17	5.10	100.00
KGR-16	Karacaören	27.83	14.83	-	3.60	35.03	12.88	-	0.23	-	0.44	0.81	4.36	100.00
KGR-5A	Karacaören	30.63	17.81	-	3.42	33.76	8.45	-	0.14	-	0.46	1.80	3.52	100.00
KGR-7A	Karacaören	24.59	17.09	-	4.06	35.88	12.47	-	0.25	-	0.51	0.75	4.41	100.00
KDG-1	Kadıncık	17.15	17.52	1.48	4.04	42.05	12.35	-	0.39	-	0.63	-	4.38	100.00
KDG-2	Kadıncık	24.04	13.80	0.76	3.56	38.42	14.71	-	0.25	-	0.47	-	3.97	99.99
GRP-1	Dinek	13.48	10.87	1.71	2.99	37.23	29.84	-	0.25	-	0.44	-	3.19	100.00
GRP-2	Dinek	16.45	13.53	2.02	3.20	43.66	16.67	-	0.25	-	0.49	-	3.73	100.00
TEK-1	Tekören	13.97	17.43	3.45	5.89	39.26	12.82	-	0.53	-	0.74	-	5.90	100.00
TEK-2	Tekören	18.85	15.76	0.21	5.29	36.05	18.26	-	0.44	-	0.53	-	4.60	99.99
KANK-1	Kadıncık	5.83	16.23	9.86	13.25	29.19	8.98	-	0.32	-	1.01	-	15.31	99.99
KGR-DY	Karacaören	-	17.84	8.80	5.47	38.16	10.93	6.10	0.56	-	1.96	-	10.16	99.99
DIY-1	Karacaören	-	18.50	10.82	1.42	37.23	9.34	9.61	0.51	-	2.01	-	10.56	100.00
DIY-2	Karacaören	-	30.07	7.67	2.64	30.72	7.09	7.98	0.46	-	1.80	-	11.58	100.00
DY-3	Karacaören	25.84	5.22	0.00	8.73	24.03	14.60	-	0.65	-	2.05	10.40	8.48	100.00

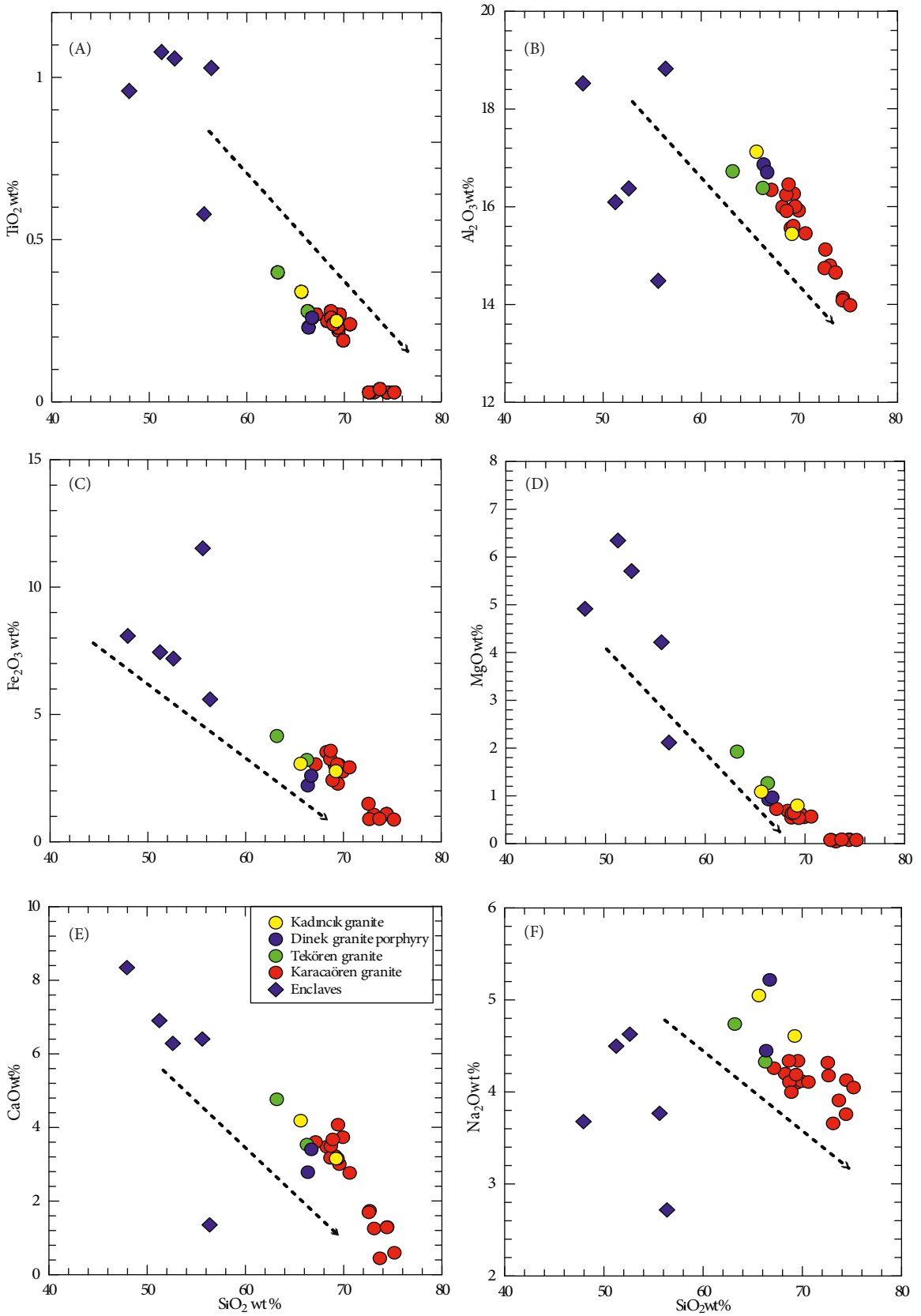

Figure 10. Selected major element (a–f) Harker diagrams of the Günyüzü Intrusive Complex.

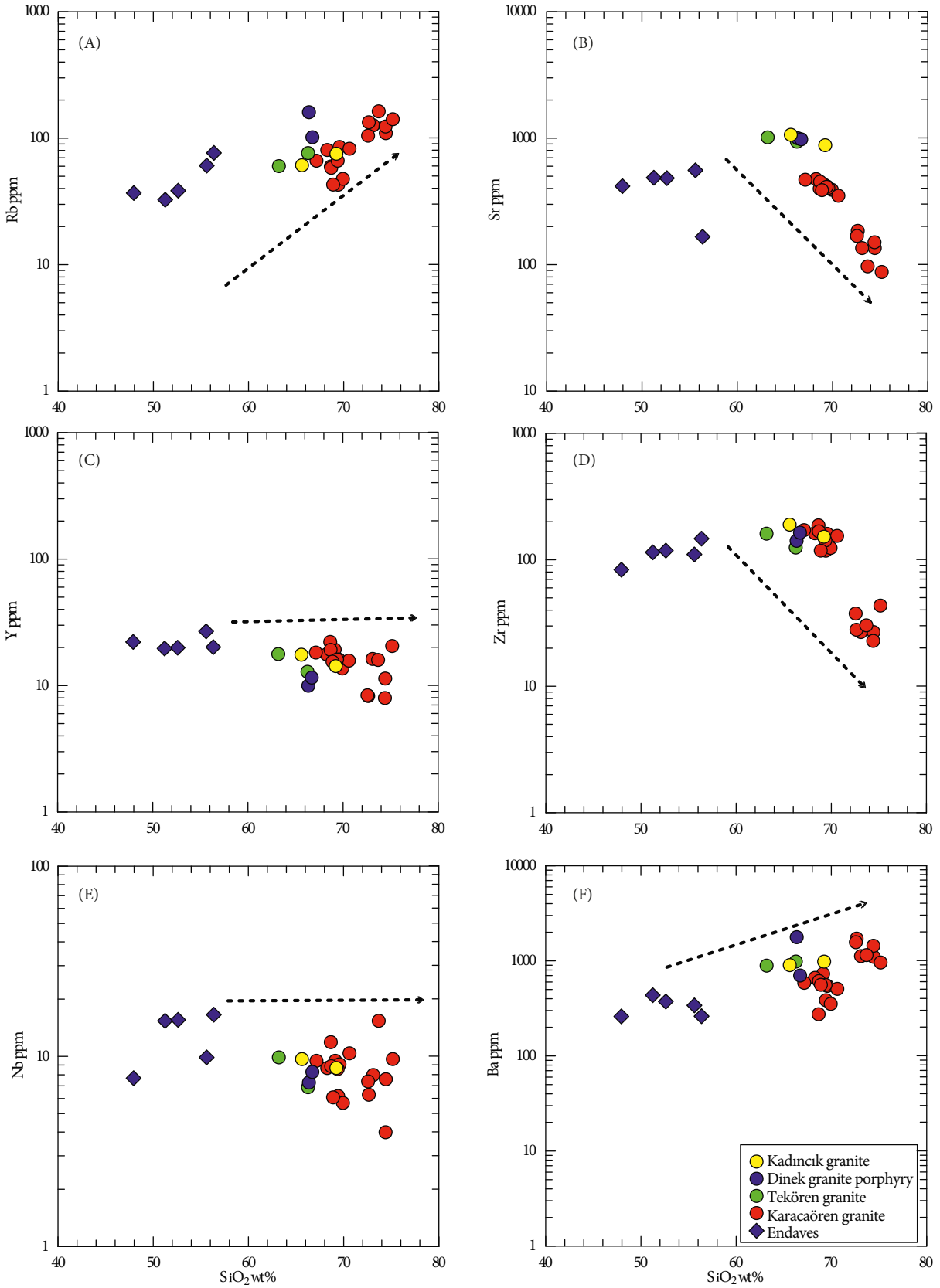

Figure 11. Selected trace element (a–f) Harker diagrams of the Günyüzü Intrusive Complex.

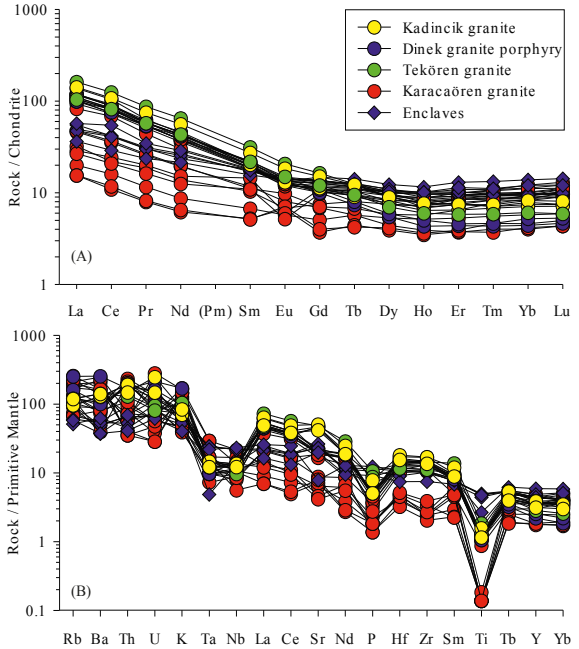

Figure 12. (a) Chondrite-normalized REE patterns of the Günyüzü Intrusive Complex. Normalization factors after Boynton (1984). (b) Primitive mantle-normalized multielement diagram of the rocks (samples >5% modal quartz are plotted). Normalizing factors after Sun and McDonough (1989).

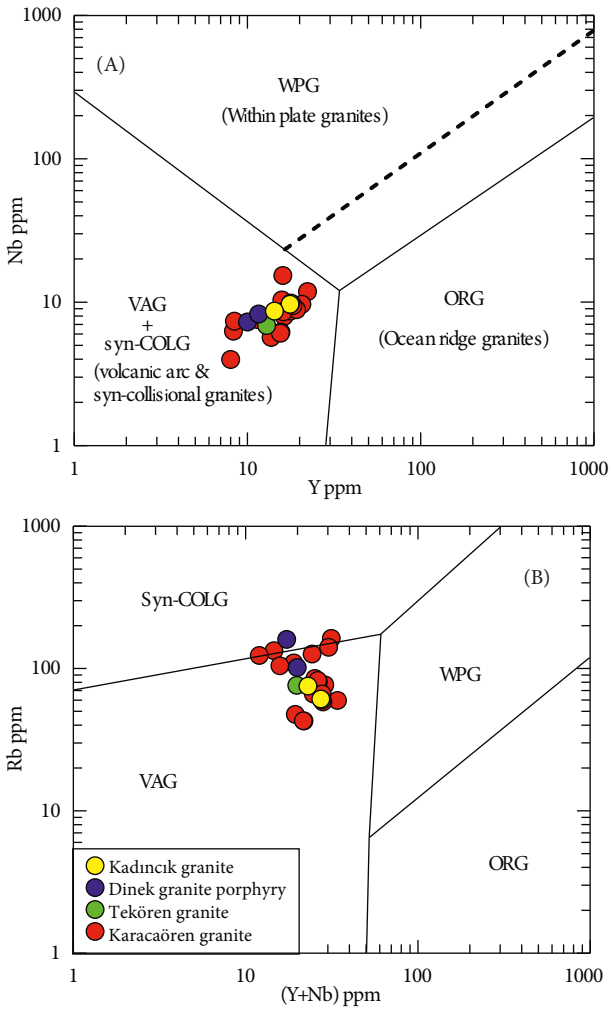

Figure 13. (a) Nb versus Y and (b) Rb versus (Y+Nb) discrimination diagrams for the Günyüzü intrusive complex (>5% modal quartz) (after Pearce et al., 1984).

the intrusive complex formed in the end of homogeneous mixing or heterogeneous mingling of the mafic and felsic magmas. It may also be noted that K-feldspar derived from potassic solutions formed as the result of nucleation/growth processes (e.g., Johnson and Glazner, 2010). Mafic and felsic minerals such as biotite, plagioclase, epidote, and titanite formed previously within the growth zone aligned (Figure 7a; Demirbilek et al., 2018). According to Hibbard (1991), this kind of texture points to magma mixing. However, alternatively, this texture appears as a closure of the small crystals, which previously formed from K-feldspar nucleation (e.g. Winkler and Schultes, 1982; Johnson and Glazner, 2010).

Considering all these conditions, the closures of mafic magma indicating magma mixing/mingling of granites, separation of K-feldspar megacrystals from potassic solutions as a result of fractional crystallization of magma, and free growth of euhedral megacrysts in the pores emphasize an active magma mixing/mingling process (e.g. Vernon, 1986). In addition to development of growth zones, textures of poikilitic K-feldspar (Figures 7a and 7b), anti-rapakivi, blade-shaped biotite (Figure 7c), and needle-like apatite indicate magma mixing/mingling (e.g., Fernandez and Barbarin, 1991; Hibbard, 1991, 1995).

Minerals such as quartz, plagioclase, biotite, titanite, apatite, and zircon observed as closures in the plagioclase are also evidence of magma mixing/mingling. The presence of lath-shaped plagioclase in the prismatic-shaped porphyritic plagioclase supports the processes of magma mixing/mingling. The existence of spongy cellular melting texture in some plagioclases is an indicator of magma mixing/mingling (Figure 7c). Kink-bands in biotites and some plagioclases of the Karacaören intrusive rocks may especially be explained by evidence of a process of subsolidus crystallization/deformation or elastic folding related to tectonism (Figures 7d and 7e).

In addition, normalized REE and multielement patterns of the enclaves are similar to those of the GIC rocks (Figures 12a and 12b). On the basis of field, petrographic, and geochemical data, partial melting of continental crust,

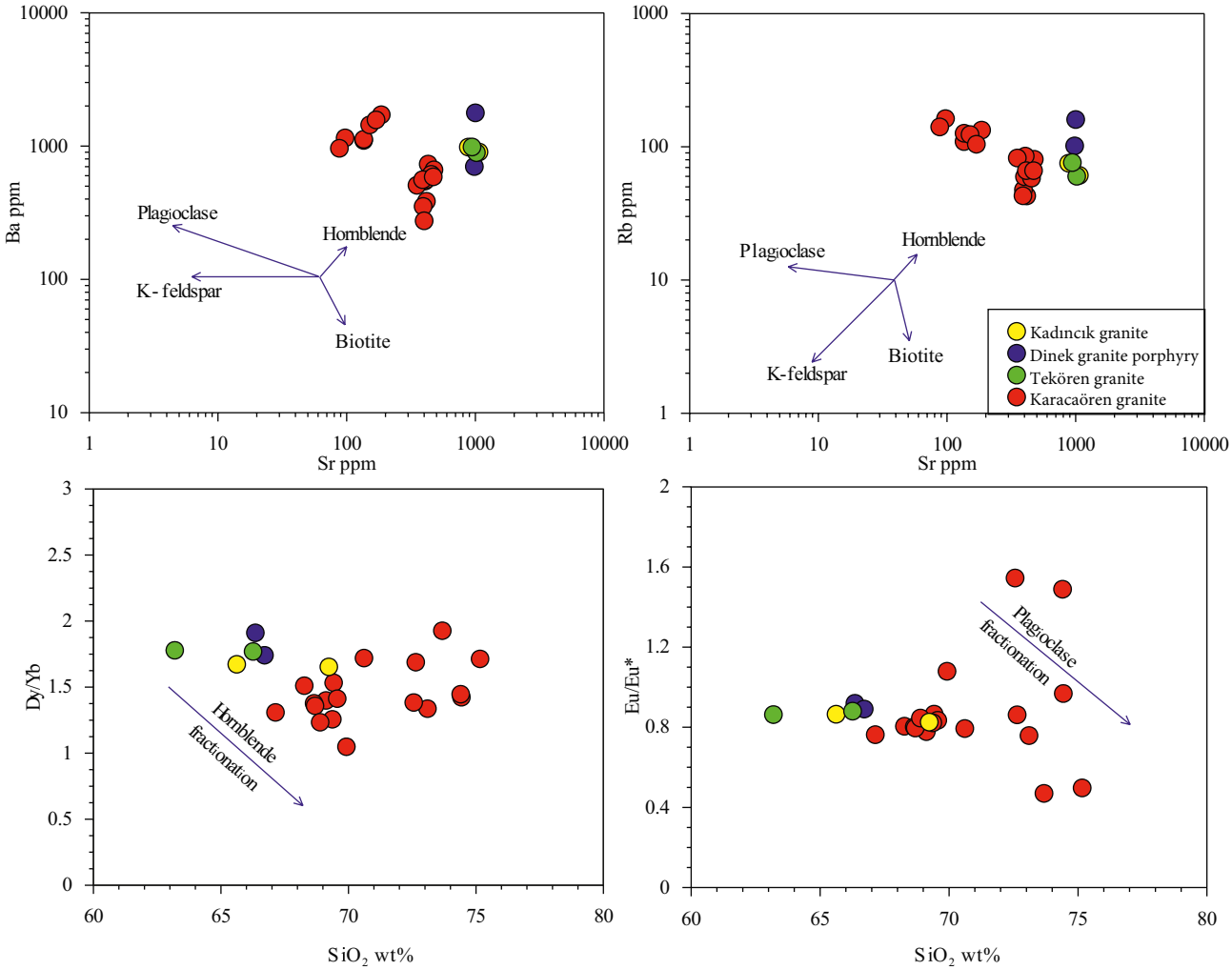

Figure 14. (a) Ba-Sr. (b) Rb-Sr. (c) Dy/Yb-SiO_2, and (d) Eu/Eu*-SiO_2 diagrams for the Günyüzü Intrusive Complex displaying fractional crystallization trends.

fractional crystallization, and/or crustal assimilation and also magma mixing/mingling were important processes in the origin of the GIC rocks.

6.2. Tectonic implications

After the collision of the Tavşanlı Zone with the Sakarya Continent along the İzmir-Ankara-Erzincan Suture Zone during the Late Cretaceous-Early Paleocene (Okay and Satır, 2006), collision-related activities finalized in the Early-Middle Eocene consisting of the emplacement of the plutons in this zone (e.g., Harris et al., 1994; Köprübaşı and Aldanmaz, 2004; Okay and Satır, 2006; Altunkaynak, 2007; Karacık et al., 2008; Altunkaynak et al., 2012a, 2012b; Demirbilek, 2012; Demirbilek et al., 2018).

In this postcollisional setting environment, main processes could induce this Eocene magmatism: subduction or slab break-off. Okay and Satır (2006) noted that the location of the subduction zone is the main problem for the former model since the Hellenic subduction zone is too far away (~700 km) from the Tavşanlı Zone (Figure 1); therefore, this model can be ruled out.

For the following reasons, slab break-off is the preferred model for the origin of the GIC: (i) the ages of the plutons in the Tavşanlı Zone are limited to Eocene times (e.g., Ataman, 1972, 1973; Cox et al., 1979; Harris et al., 1994; Sherlock et al., 1999; Okay and Satır, 2006; Shin et al., 2013; Demirbilek et al., 2018; this study) (Table 3); (ii) the Eocene plutons in the Tavşanlı Zone are restricted to just south of the İzmir-Ankara-Erzincan Suture Zone (Figure 2).

In addition, the plutons in the zone are, in line, parallel to the suture zone trending NW-SE (Figure 2). Okay and Satır (2006) and Shin et al. (2013) suggested that slab break-off took place at greater than 80 km in depth and occurred in the latest Cretaceous (~70 Ma). Altunkaynak (2007) also suggested a slab break-off model for the ori-

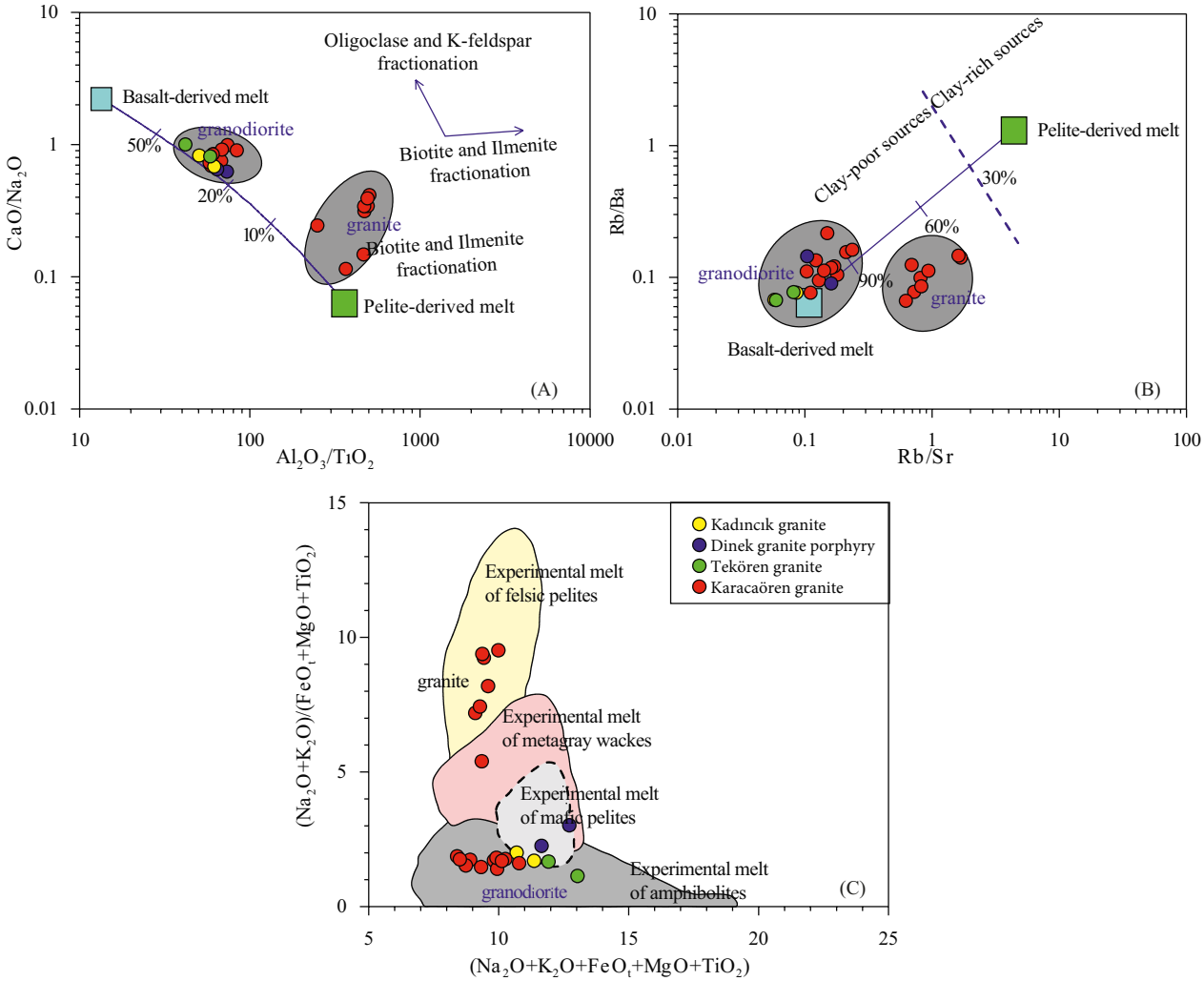

Figure 15. (a) CaO/Na_2O versus Al_2O_3/TiO_2; (b) Rb/Ba versus Rb/Sr (the mixing curve between basalt- and pelite-derived melt is from Sylvester, 1998); and (c) $(Na_2O+K_2O)/(FeO_t+MgO+TiO_2)$ versus $(Na_2O+K_2O+FeO_t+MgO+TiO_2)$ diagrams for the Günyüzü Intrusive Complex.

gin of the Eocene plutons located to north of the İzmir-Ankara-Erzincan Suture Zone.

The geochemical results indicate that the GIC from the Tavşanlı Zone could have been generated through initially subduction and later collision-related and slab break-off processes (Figure 16). The latter led to asthenospheric upwelling and partial melting of subduction-enriched subcontinental lithospheric mantle melts involved in magma mixing/mingling process. The origin of high-K calc-alkaline and shoshonitic plutons may have been derived from these melts (Figure 16).

7. Conclusions

(i) The Rb-Sr whole-rock dating indicates that the GIC (Karacaören, Tekören, Dinek, Kadıncık) in the Tavşanlı Zone emplaced at 47.0 ± 1.0 to 40.8 ± 3.0 Ma. Thus, this magmatism took place after the continent–continent collision.

(ii) The plutonic rocks have metaluminous to peraluminous, medium-K calc-alkaline to shoshonitic, and I-type granite characteristics. They are mainly granodiorite to granite in composition.

(iii) The GIC has mafic enclaves showing MMEs characteristics. The host and their MMEs have similar mineral assemblages and geochemical characteristics, related to magma mixing/mingling.

(iv) All intrusive rocks from the zone are enriched in LILEs and depleted in HFSEs, indicating features of subduction-related intrusive rocks.

(v) The geochemical data reveal that the intrusive rocks are derived mainly from partial melting of mafic crustal sources. Not only partial melting but also fractional

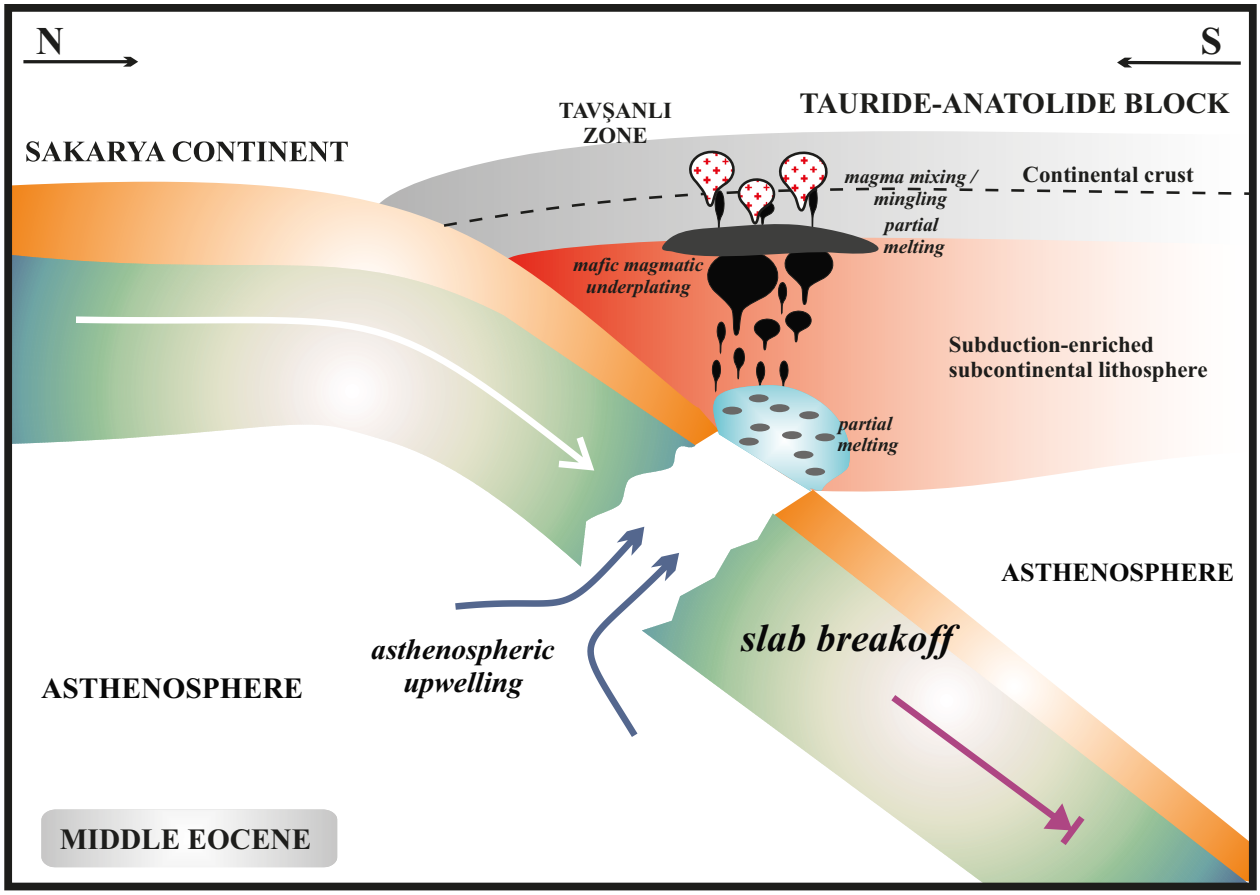

Figure 16. Diagram illustrating the production of the Günyüzü Intrusive Complex responding to slab break-off in the Middle Eocene.

crystallization and magma mixing/mingling were also important processes for the evolution of parental magmas. (vi) The source of magmas for the GIC probably originated from slab break-off causing partial melting of subduction-enriched lithospheric mantle.

Acknowledgments

This work was part of a research project supported by Afyon Kocatepe University (08.ISCMYO.02.). The authors are grateful for the supportive comments of all anonymous reviewers.

References

Altherr R, Holl A, Hegner E, Langer C, Kreuzer H (2000). High-potassium, calc-alkaline plutonism in the European Variscides: northern Vosges (France) and northern Schwarzwald (Germany). Lithos 50: 51-73.

Altunkaynak S (2007). Collision-driven slab breakoff magmatism in northwestern Anatolia, Turkey. J Geol 115: 63-82.

Altunkaynak S, Dilek, Y, Genç SC, Sunal, G, Gertisser R, Furnes H, Foland KA, Yang J (2012a). Spatial, temporal and geochemical evolution of Oligo–Miocene granitoid magmatism in western Anatolia, Turkey. Gondwana Res 21: 961-986.

Altunkaynak S, Sunal G, Aldanmaz E, Genç SC, Dilek Y, Furnes H, Foland KA, Yang J, Yıldız M (2012b). Eocene granitic magmatism in NW Anatolia (Turkey) revisited: new implications from comparative zircon SHRIMP U-Pb and 40Ar-39Ar geochronology and isotope geochemistry on magma genesis and emplacement. Lithos 155: 289-309.

Ataman G (1972). The radiometric age of the Orhaneli granodiorite. Bull Geol Soc Turkey 15: 125-130 (in Turkish).

Ataman G (1973). The radiometric age of the Gürgenyayla (Domanic) granodiorite. Bull Geol Soc Turkey 16: 22-26 (in Turkish).

Bağcı M, Kibici Y, Yıldız A, İlbeyli N, Gürcan S, Demirbilek M, Dumlupunar İ (2011). The Mineralogical Properties of Granitic Rocks from Günyüzü (Sivrihisar, Eskişehir), and Investigation of Isotope Geochemistry and Physique-Mechanical Properties. Project No: 08.ISCMYO.02. Afyonkarahisar, Turkey: Coordinatorship of Scientific Research Project of Afyon Kocatepe University (in Turkish).

Barbarin B (1992). Les granites crustaux hercyniens d'Europe Occidentale. Comparaison avec les granites S du Lachlan Fold Belt, Australie. Dualité d'origine. C R Acad Sci 314: 595-601 (in French).

Boynton WV (1984). Geochemistry of the Rare Earth Elements: Meteorite Studies. In: Henderson P, editor. Rare Earth Element Geochemistry. Amsterdam, the Netherlands: Elsevier, pp. 63-114.

Chappell BW, White AJR (1974). Two contrasting granite types. Pacific Geology 8: 173-179.

Clarke DB (1992). Granitoid Rocks. New York, NY, USA: Chapman and Hall.

Clemens JD, Wall, VJ (1981). Origin and crystallization of some peraluminous (S-type) granitic magmas. Canadian Mineralogist 9: 111-131.

Çoğulu E, Krummenacher D (1967). Problemes geochronome triques danslepartie NW del'Anatolie Centrale (Turquie). Schweiz Mineral Petrogr Mitt 47: 825-831 (in French).

Cox KG, Bell JD, Pankhurst RJ (1979). The Interpretation of Igneous Rocks. London, UK: George, Allen and Unwin.

Delaloye M, Bingöl E (2000). Granitoids from western and northwestern Anatolia: Geochemistry and modeling of geodynamic evolution. Int Geol Rev 42: 241-268.

Demirbilek M (2012). Geochemical, geochronological and isotopic constraints on the intrusive rocks in the Günyüzü, Sivrihisar and Kaymaz regions (Eskişehir). PhD, Osmangazi University, Eskişehir, Turkey (in Turkish).

Demirbilek M, Mutlu H (2012). Geochemical, geochronologic and Sr/Nd isotopic characteristics of the late Paleocene-Middle Eocene granitoids in the Tavşanlı zone, NW Turkey. In: Candan O, Çolak M, editors. International Earth Science Colloquium on the Aegean Region (IESCA), pp. 210-211.

Demirbilek M, Mutlu H, Fallick AE, Sarıız K, Kibici Y (2018). Petrogenetic evolution of the Eocene granitoids in eastern part of the Tavşanlı Zone in northwestern Anatolia, Turkey. Lithos 314-315: 236-259.

Didier J (1973). Granites and Their Enclaves: The Bearing of Enclaves on the Origin of Granites. Amsterdam, the Netherlands: Elsevier.

Dilek Y, Thy P, Hacker B, Grundvig S (1999). Structure and petrology of Tauride ophiolites and mafic dike intrusions (Turkey): implications for the Neotethyan Ocean. Geol Soc Am Bul 111: 1192-1216.

Fernandez AN, Barbarin B (1991). Relative rheology of coeval mafic and felsic magmas: nature of resulting interaction processes. Shape and mineral fabric of mafic microgranular enclaves. In: Didier J, Barbarin B, editors. Enclaves and Granite Petrology. Amsterdam, the Netherlands: Elsevier, pp. 263-276.

Gardien V, Thompson AB, Grujic D, Ulmer P (1995). Experimental melting of biotite-plagioclase-quartz-muscovite assemblages and implications for crustal melting. J Geophys Res 100: 15581-15591.

Gautier Y (1984). Deformation et metamorfismes associes a la suture Tethysienno en Anatolie centrale (Region de Sivrihisar, Turquie). PhD, University of Paris Sud, Orsay, France (in French).

Harris NBW, Kelley SP, Okay AI (1994). Postcollision magmatism and tectonics in northwest Turkey. Contrib Mineral Petrol 117: 241-252.

Hibbard MJ (1991). Textural anatomy of twelve magma-mixed granitoid systems. In: Didier J, Barbarin B, editors. Enclaves and Granite Petrology. Amsterdam, the Netherlands: Elsevier, pp. 431-444.

Hibbard MJ (1995). Petrography to Petrogenesis. New York, NY, USA: Prentice Hall.

İlbeyli N, Kibici Y (2009). Collision-related magma genesis, their potential source and tectono-magmatic evolution: comparison between central, northwestern and western Anatolia (Turkey). Int Geol Rev 51: 252-278.

Johnson RB, Glazner FA (2010). Formation of K-feldspar megacrysts in granodioritic plutons by thermal cycling and late-stage textural coarsening. Contrib Mineral Petrol 159: 599-619.

Jung S, Hoernes S, Mezger K (2000). Geochronology and petrogenesis of Pan-African, syn-tectonic, S-type and post-tectonic A-type granite (Namibia): products of melting of crustal sources, fractional crystallization and wall rock entrainment. Lithos 50: 259-287.

Karacık Z, Tüysüz (2010). Petrogenesis of the Late Cretaceous Demirköy igneous complex in NW Turkey: implications for magma genesis in the Strandja Zone. Lithos 114: 369-384.

Karacık Z, Yılmaz Y, Pearce J, Ece Ö (2008). Petrochemistry of the south Marmara granitoids, northwest Anatolia, Turkey. International Journal of Earth Sciences 97: 1181-1200.

Kibici Y (1994). Geochemical properties and genetical interpretation of the igneous rocks in Sivrihisar-Günyüzü (Eskişehir). Çukurova University Geosound 25: 1-12 (in Turkish).

Kibici Y, Dağ N, Özgenç I (1993). Mineralogical and petrographical properties of the Sivrihisar-Günyüzü (Eskişehir) granitoid belt. Çukurova University Geosound 23: 97-112 (in Turkish).

Kibici Y, İlbeyli N, Yıldız A, Bağcı M (2008). Geochemical Constraints on the genesis of the Günyüzü pluton, Northwest Anatolia, Turkey. Int Geol Rev 50: 931-947.

Köprübaşı N, Aldanmaz E (2004). Geochemical constraints on the petrogenesis of Cenozoic I-type granitoids in northwestern Anatolia, Turkey: evidence for magma generation by lithospheric delamination in a post-collisional setting. Int Geol Rev 46: 705-729.

Kumar S, Rino V (2006). Mineralogy and geochemistry of microgranular enclaves in Palaeoproterozoic Malanjkhand granitoids, central India: evidence of magma mixing, mingling, and chemical equilibration. Contrib Mineral Petrol 152: 591-609.

Lefebvre C, Meijers MJM, Kaymakci N, Peynircioğlu A, Langereis CG, Van Hinsbergen DJJ (2013). Reconstructing the geometry of central Anatolia during the late Cretaceous: large-scale Cenozoic rotations and deformation between the Pontides and Taurides. Earth Planet Sci Lett 366: 83-98.

Lisenbee A (1972). Structural setting of the Orhaneli ultramafic massif near Bursa, Northwestern Turkey. PhD, Pennsylvania State University, State College, PA, USA.

Ludwig KR (2003). Isoplot 3.0: A geochronological toolkit for Microsoft Excel. Berkeley Geochron Cent Spec Publ 4: 1-70.

Meijers MJM, Langereis CG, van Hinsbergen DJJ, Kaymakcı N, Stephenson RA, Altıner D (2010). Jurassic-Cretaceous low paleolatitudes from the circum Black Sea region (Crimea and Pontides) due to True Polar Wander. Earth Planet Sci Lett 296: 210-226.

Middlemost EAK (1994). Naming materials in the magma/igneous rock system. Earth-Sci Rev 37: 215-224.

Okay AI (1984). Distribution and characteristics of the northwest Turkish blueschists. In: Dixon JE, Robertson AHF, editors. The Geological Evolution of the Eastern Mediterranean. London, UK: Geological Society of London Special Publications, pp. 455-466.

Okay AI (2002). Jadeite-chloritoid-glaucophane-lawsonite schists from northwest Turkey: unusually high P/T ratios in continental crust. J Met Geol 20: 757-768.

Okay AI (2008). Geology of Turkey: a synopsis. Anschnitt 21: 19-42.

Okay AI, Harris NBW, Kelley SP (1998). Exhumation of blueschists along a Tethyan suture in northwest Turkey. Tectonophysics 285: 275-299.

Okay AI, Satır M (2006). Geochronology of Eocene plutonism and metamorphism in northest Turkey: evidence for a possible magmatic arc. Geo Acta 19: 251-266.

Okay AI, Tüysüz O (1999). Tethyan sutures of northern Turkey. In: Durand B, Jolivet L, Hovarth F, Séranne M, editors. The Mediterranean Basins: Tertiary Extension within the Alpine Orogen Tethyan Sutures of Northern Turkey. London, UK: Geological Society of London Special Publications, pp. 475-515.

Önen P (2003). Neotethyan ophiolitic rocks of the Anatolides of NW Turkey and comparison with Tauride ophiolites. J Geol Soc 160: 947-962.

Patīno Douce AE (1996). Effects of pressure and H_2O contents on the composition of primary crustal melts. Trans R Soc Edinburgh Earth Sci 87: 11-21.

Patīno Douce AE (1999). What do experiments tell us about the relative contributions of crust and mantle to the origin of granitic magmas? In: Castro A, Fernandez C, Vigneressese JL, editors. Understanding Granites: Integrating New and Classical Techniques. London, UK: Geological Society of London Special Publications, pp. 55-75.

Patīno Douce AE, Beard JS (1995). Dehydration melting of biotite gneiss and quartz amphibolite from 3to 15 kbar. J Petrol 36: 707-738.

Patīno Douce AE, Beard JS (1996). Effects of P, f(O2) and Mg/Fe ratio on dehydration melting of model metagreywackes. J Petrol 37: 999-1024.

Patīno Douce AE, McCarthy TC (1998). Melting of crustal rocks during continental collision and subduction. In: Hacker BR, Liou JG, editors. When Continents Collide: Geodynamics and Geochemistry of Ultrahigh-Pressure Rocks. Dordrecht, the Netherlands: Kluwer Academic Publishers, pp. 27-55.

Pearce JA, Harris NBW, Tindle AG (1984). Trace element discrimination diagrams for the tectonic interpretation of granitic rocks. J Petrol 25: 956-983.

Perugini D, Poli G (2012). The mixing of magmas in plutonic and volcanic environments: Analogies and differences. Lithos 153: 261-277.

Poli G, Tommasini S (1991). Model of the origin and significance of microgranular enclaves in calc-alkaline granitoids. J Petrol 32: 657-666.

Reid JB Jr, Evans OC, Fates DG (1983). Magma mixing in granitic rocks of the central Sierra Nevada, California. Earth Planet Sci Lett 66: 243-261.

Rickwood PC (1989). Boundary lines within petrologic diagrams which use oxides of major and minor elements. Lithos 22: 247-263.

Seaton NCA, Whitney DL, Teyssier C, Toraman E, Heizler MT (2009). Recrystallization of high-pressure marble (Sivrihisar, Turkey). Tectonophysics 479: 241-253.

Şengör AMC, Yılmaz Y (1981). Tethyan evolution of Turkey: a plate tectonic approach. Tectonophysics 75: 181-241.

Şengör AMC, Yılmaz Y, Ketin İ (1982). Remnants of a pre-Late Jurassic ocean in northern Turkey, Fragments of Permo-Triassic Paleo-Tethys. Reply. Geol Soc Am Bull 93: 932-936.

Sherlock S, Kelley SP, Inger S, Harris N, Okay AI (1999). ^{40}Ar-^{39}Ar and Rb-Sr geochronology of high-pressure metamorphism and exhumation history of the Tavsanli Zone, NW Turkey. Contrib Mineral Petrol 137: 46-58.

Shin T, Catlos E, Jacob L, Black K (2013). Relationships between very high pressure subduction complex assemblages and intrusive granitoids in the Tavşanlı Zone, Sivrihisar Massif, central Anatolia. Tectonophysics 595-596: 183-197.

Singh J, Johannes W (1996). Dehydration melting of tonalites: Part II. Composition of melts and solids. Contrib Mineral Petrol 125: 26-44.

Streckeisen A, Le Maitre RW (1979). A chemical approximation to the modal QAPF classification of the igneous rocks. N Jb Mineral Abh 136: 169-206.

Sun SS, McDonough WF (1989). Chemical and isotopic systematics of oceanic basalts: implications for mantle composition and processes. In: Saunders AD, Norry MJ, editors. Magmatism in the Ocean Basins. London, UK: Geological Society of London Special Publications, pp. 313-345.

Sylvester PJ (1998). Post-collisional strongly peraluminous granites. Lithos 45: 29-44.

Tekin UK, Göncüoğlu MC, Turhan N (2002). First evidence of Late Carnian radiolarians from the Izmir-Ankara suture complex, central Sakarya, Turkey: implications for the opening age of the Izmir-Ankara branch of Neo-Tethys. Geobios 35: 127-135.

Thompson AB (1996). Fertility of crustal rocks during anatexis. Trans R Soc Edinburgh Earth Sci 87: 1-10.

Tüysüz O, Dellaloğlu AA, Terzioğlu N (1995). A magmatic belt within the Neo-Tethyan suture zone and its role in the tectonic evolution of northern Turkey. Tectonophysics 243: 173-191.

Vernon RH (1983). Restite, xenoliths and microgranitod enclaves in granites. J Proc R Soc New South Wales 116: 77-103.

Vernon RH (1984). Microgranitoid enclaves: globules of hybrid magma quenched in a plutonic environment. Nature 304: 438-439.

Vernon RH (1986). K-feldspar megacrysts in granites; phenocrysts, not porphyroblasts. Earth Sci Rev 23: 1-63.

Vernon RH (2014). Microstructures of microgranitoid enclaves and the origin of S-type granitoids. Aust J Earth Sci 61: 227-239.

Vernon RH, Etheridge ME, Wall VJ (1988). Shape and microstructure of microgranitoid enclaves: indicators of magma mingling and flow. Lithos 22: 1-11.

Wang J, Hattori KH, Kilian R, Stern CR (2007). Metasomatism of sub arc mantle peridotites below southernmost South America: Reduction of SiO_2 by slab-melt. Contrib Mineral Petrol 153: 607-624.

Winkler HGF, Schultes H (1982). On the problem of alkali feldspar phenocryst in granitic rocks. N Jb Mineral Monatsh 12: 558-564.

Wolf MB, Wyllie PJ (1994). Dehydration-melting of amphibolite at 10 kbar: Effects of temperature and time. Contrib Mineral Petrol 115: 369-383.